scientific reports

Check for updates

OPEN

An innovative modelling technique for bimodal soil water characteristic curve under wetting process

Nura Bello[1], Alfrendo Satyanaga[1]✉, Sonny Irawan[2], Qian Zhai[3,5], Nurly Gofar[4] & Jong Kim[1]

Accurate measurement and use of an appropriate soil-water characteristics curve (SWCC) is crucial because it underpins most other estimations and analyses in unsaturated soil mechanics. Since it is difficult to measure a complete SWCC in the laboratory without combining multiple test methods, mathematical equations are subsequently used to model the SWCC that covers the entire suction range (up to 10^6 kPa). Studies have been carried out to develop mathematical equations for modelling drying bimodal SWCC. However, no equations have been developed to model bimodal SWCC under wetting process. Ignoring the wetting SWCC could lead to results which do not represent the actual condition of the soil, especially under water infiltration due to rainfall and snowmelt. This is coupled with the fact that all available best-fitting equations are either complex and cumbersome or have parameters lacking physical meaning in relation to the variables of SWCC. In this paper, a new mathematical equation is proposed to model the bimodal SWCC under wetting process. Several experimental datasets from published literature were used to assess the performance of the proposed equation. The results of the statistical analysis indicate that the coefficient of determination (R^2) is close to 1.0 and root mean square error (RMSE) is approaching 0. In addition, an approach to measure hysteresis of SWCC using high suction polymer sensor (HSPS) has been developed, although this can be made using other methods such as pressure plate. However, this method is fast and can measure the bimodal SWCC under wetting process accurately, which is a novel method on the topic. It should be noted that all the parameters in the proposed model have physical meaning, and the proposed equation has its advantage in representation of the bimodal SWCC under wetting process.

Keywords Unsaturated soil, Wetting curve, Bimodal soil, High Suction polymer sensor, Exponential function

Soil shear strength, factor of safety of slope stability and bearing capacity of shallow foundation are affected by drying (e.g., due to evaporation) and wetting (e.g., due to precipitation) of the soil[1]. The soil-water characteristics curve (SWCC) is an important parameter representing the relationship between the amount of water in the soil's pores and the soil suction. The SWCC could effectively be utilized in estimating other unsaturated soil properties, such as unsaturated coefficient of permeability, unsaturated shear strength and unsaturated tensile strength[2–5]. It could also be used in modelling unsaturated soil behavior, such as in seepage and slope stability analyses[5–8].

Researchers such as Kristo and Rahardjo[9], Qi, et al.[10]and Rahardjo and Satyanaga[11] have noted that an increase in temperature causes a rise in moisture content in the atmosphere, leading to an increase of intense rainfall across the globe. The areas with such high rainfall and protracted dry seasons are often linked with rainfall-induced landslides. Since most landslides occur within the unsaturated part of the soil. A thorough unsaturated transient seepage analysis that encompasses the actual nature of the soil, and all the moisture conditions and

[1]Department of Civil and Environmental Engineering, School of Engineering and Digital Sciences, Nazarbayev University, Kabanbay Batyr Ave., 53, 010000 Nur-Sultan, Kazakhstan. [2]Department Petroleum Engineering, School of Mining and Geosciences, Nazarbayev University, Kabanbay Batyr Ave., 53, 010000 Nur-Sultan, Kazakhstan. [3]School of Civil Engineering, Southeast University, Jiangsu, Nanjing 211189, China. [4]Department of Civil Engineering, Post Graduate Program, Universitas Bina Darma, Palembang 30111, Indonesia. [5]Advanced Ocean Institute of Southeast University, Southeast University, Jiangsu, Nantong 226010, China. ✉email: alfrendo.satyanaga@nu.edu.kz

their effects on the soil is necessary. This is particularly important in the assessment of cyclic-rainfall influence, designs of slopes, and other geotechnical structures on unsaturated soils.

SWCC is hysteretic in nature as shown by many researchers such as[4,12–15]. By being hysteretic, it means wetting and drying paths of SWCC are different[14]. The hysteresis is caused by several factors, such as ink-bottle effect, entrapped air and/or contact angle difference during soil drying and wetting, and in many instances, the cyclic wetting and drying history of the soil[16,17]. In essence, there are always two main boundary curves representing drying SWCC and wetting SWCC. This behavior is being used by researchers in transient seepage analysis to model effects of rainfall in soil. Wetting SWCC, which represents soil wetting, is certainly more relevant to practical problems than the drying curve since majority of failures of geotechnical structures occur during soil wetting.

Several soil types, such as gap-graded soils, compacted soils in transportation pavements, compacted coarse colluvial soils, coarse colluvial soils with high coarse fraction commonly have dual porosity structure[18,19]. These types of soil are usually associated with bimodal grain size distribution and bimodal SWCC. This is attributed to their unique property of having two dominant pore sizes family, the micropores and macropores[20]. The soil pore structure is believed to be the most important factor influencing soil moisture flow, directly controlling important soil functional characteristics such as soil hydraulic properties[21,22].

Previous studies by Syarifudin and Satyanaga[23]indicated that the dual structural soil maintained its structure stable during heavy rainfall. This is because the infiltrated water can drain out easily through its macropores. As a result, the dual structural soil is favorable for use in practical engineering where too much water retention is not entirely needed[24–26]. For this reason, this soil type should be critically investigated and fully understood.

SWCC forms the basis of estimating other unsaturated soil's properties, and it is the most important input parameter in the transient seepage analysis[27,28]. It is then important to use the relevant and appropriate SWCC that represents actual soil conditions in all work. In particular, it is imperative to consider hysteresis of SWCC in the seepage analysis for the scenarios that involve both drying and wetting conditions of the soil.

Due to the hysteresis of SWCC, at the same suction value, moisture content is higher during drying than during wetting. Hysteresis affects all unsaturated soil's properties, particularly when the SWCC is used in estimating the properties. Measurement of wetting SWCC is difficult and time consuming. Therefore, researchers usually neglect the hysteresis of SWCC and use only drying curve in modelling both soil drying and soil wetting. This usually leads to inaccurate estimations and analyses that do not represent the exact soil's conditions.

There are a variety of devices for soil suction measurements in the laboratory. There are direct suction measurements using tensiometers or axis translation-based apparatus. And there are indirect suction test apparatus using contact filter paper or using chilled mirror potentiometer that measures the relative humidity of air around soil sample[29,30]. However, the common limitation of the available devices and methods is that they could not measure the suction up to 10^6kPa with required accuracy[29]. Moreover, only a limited number of discrete data points could be obtained from the experimental measurement. Mathematical equations are commonly used to best fit those discrete data points and provide a continuous description of SWCC for the entire suction range. This is more important in bimodal SWCC where the second sub-curve's parameters usually occur in the area of high suction that are very difficult to measure in the laboratory. For example, in situations where high air entry value (or second water saturation points) is encountered, obtaining those parameters directly will help in utilizing them during modelling and analyses. Similarly, water-entry value which (can be obtained only from wetting SWCC) is very important parameter in modelling capillary barrier effect[31]. In fact, Rahardjo et al. (2007) reported that for a capillary barrier to be effective, the ratio between water-entry values of the fined-grained and coarse-grained materials should be above 10. Therefore, obtaining the variables directly would help in their accurate applications in analyses such as in modelling capillary barrier effects and Geobarrier System (GBS).

Several mathematical equations, as reviewed by Bello, et al.[32], are available for modelling both unimodal SWCC such as[2,33–38], and bimodal SWCC such as[39,40]. Most of these equations are performing well as compared with the experimental data in literature. However, the parameters in these equations are lacking physical meaning in relation to the variables of SWCC.

In particular, available models for drying bimodal SWCC such as Burger and Shackelford[20], Gitirana Jr and Fredlund[33], Zhang and Chen[40]and Li and Vanapalli[41] etc. are generally complex, and their applications are cumbersome. These models also contain mathematical characters that are just fitting parameters with no physical meaning in relation to the variables of the curve. Whilst these models can be adopted to best-fit wetting curve, there is no physical relation between their parameters and the variables of the wetting curve. Therefore, it is important to propose a model whose apart from being simple in its application, it also constitutes meaningful parameters in relation to the variables of the bimodal wetting SWCC. There are number of important SWCC variables related to the wetting SWCC such as water saturation point, delimiting point, and water entry point. If these variables of wetting curve could be readily obtained directly from a model, it would significantly simplify the model application. Physically meaningful parameters linked to variables of the bimodal wetting SWCC have several advantages. They help to directly enhance understanding of how water interacts with soil under wetting conditions. They equally help in easier parameter interpretability, reduce empirical assumptions, simplify calibration and optimization among other things. There are already a large number of literature studies on moisture absorption curves, yet available literature on moisture absorption curve for soil with dual porosity (with bimodal SWCC and bimodal pore size distribution) is still very scarce in the literature.

In addition, those bimodal SWCC equations are proposed mainly for the drying not for the wetting SWCC. Moreover, as mentioned before, using equations meant for modelling drying curve to model wetting SWCC may constitute misrepresentation of data and lead to unsound or inaccurate results. It is then necessary to have a mathematical equation that could appropriately model a bimodal wetting SWCC.

There are several studies confirming the veracity of modelling water infiltration using wetting SWCC instead of using the drying curve. For example, works such as Tami, et al.[42] show that results of numerical analyses using wetting hydraulic properties (i.e. SWCC and unsaturated permeability function) always matches well and better with the measured data using the physical model of precipitation. Likewise, Rahardjo, et al.[31] utilized hysteresis behavior of unsaturated hydraulic properties to model the effects of rainfall deformation of geobarrier, these helps in attaining more realistic results as per their report. Similarly, Kristo et al.[9], conducted three different numerical seepage and stability analyses on a soil slope subject to wetting and drying. The analyses considered (i) only drying SWCC (ii) only wetting SWCC, and (iii) combined wetting and drying SWCC. The results of the analyses indicated that those obtained by combining both drying and wetting SWCCs are closer and in agreement with those considering only wetting SWCC than those considering only drying SWCC. In general, the study concluded that, results obtained by incorporating only drying SWCC gave the most conservatives factor of safeties despite rainfall intensity.

Despite the importance of wetting bimodal SWCC in modelling soil wetting due to rainfall, and the application of its variables in practical applications, there are no equations to the Authors' knowledge that have been developed to model wetting bimodal SWCC.

In this paper, a mathematical equation is proposed to model the wetting bimodal SWCC for the entire suction range. In addition, a novel approach to measure wetting SWCC using high suction polymer sensor (HSPS) has been developed and it is proven that this method is fast and is capable of measuring the wetting SWCC accurately.

Proposed equation for the bimodal wetting SWCC

Theory

Hysteresis of SWCC is caused primarily by four factors: The entrapped air within the soil pores, the swelling and the shrinkage history of the soil, the effects of contact angle, and the ink-bottle effects[12,16]. The mechanism of entrapped air is associated with air bubbles that are trapped in the soil pores and reduce the amount of moisture re-entry during wetting. The water volume becomes less, even at the same applied suction; hence hysteresis occurs. For the swelling and shrinkage effects, during wetting (particularly in fine grain soil), soil particles swell and occupy parts of the pore spaces[43]. During drying, the particles shrink and create more spaces to be filled with water, and these lead to more moisture in soil pores during drying than during wetting at the same applied suction. Hysteresis may also happen due to the effects of meniscus contact angle. Contact angle is usually larger in advancing (wetting condition) than in receding (drying condition). A bigger contact angle creates a bigger radius of curvature of the meniscus. Moisture in soil is basically controlled by two distinct forces, force of cohesion between the water molecules and force of adhesion between water molecules and soil particles. Therefore, a bigger radius of curvature during wetting for a given water content is usually associated with a more dominant cohesive force, and the water molecules are more attractive to each other causing higher permeability. As compared to bigger radius, smaller radius of curvature (during drying) corresponds to a more dominant adhesive force. As a result, the water molecules are attracted to the soil particles, leading to a higher moisture content within the soil pores[17]. The ink-bottle effect is associated with a variation of soil pore sizes. The area between two pores with varying sizes (neck) play an important role as to the amount of suction needed to push moisture to and from individual pores during drying and wetting.

But as compared to other causes of hysteresis such as entrapped air, the effects of "ink-bottle" are dynamic and depends on the probability of pore connections. Therefore, while the effects of entrapped air should always be considered when modelling hysteresis, the ink-bottle effects can be assumed insignificant if the soil suction is low[44].

Pham, et al.[16]used a simple scaling method to approximate the hysteresis of SWCC, utilizing the Feng and Fredlund[45]'s equation with few modifications. They used hysteresis factors to define the two boundary curves in the calculation of the curve fitting parameters of the wetting curve. The relevant hysteresis factors are related to the distance between the two curves and the ratio of their slopes. This work utilized same procedure used in Pham, et al.[16] and Satyanaga, et al.[13] to develop an equation for modelling bimodal wetting curve.

Exponential function is one of the fundamental mathematical concepts widely utilized in modelling real-life phenomena both in the scientific and social field. It provides a unique means to link the important gap between mathematical theories and physical attributes[46].

This work utilized the similarity of the SWCC with a graph of reciprocal of exponential function having a value range of 0–1.

Figure 1a and b could be related by equating the reciprocal of exponential function of matric suction "equation (1)" to normalized volumetric water content (Θ) "equation (2)". Equation (1) used an exponential function to model SWCC just in the same way McKee and Bumb (1984) used the Boltzman distribution.

$$\Theta = \exp\left[-\mathrm{F}(\psi)\right] \tag{1}$$

$$\Theta = \frac{\theta - \theta_{min}}{\theta_{max} - \theta_{min}} \tag{2}$$

where (θ_{max}) is related to water content at saturation, (θ_{min}) is water content at water entry point, while (θ) is calculated water content corresponding to a particular suction (ψ).

The function $\mathrm{F}(\psi)$ is equal to zero at suction below the water saturation point and valid all through the curve length at any suction beyond water saturation point as shown in Eq. (3) and Eq. (4) respectively.

$$\mathrm{F}(\psi) = 0; \text{ when } (\psi) < (\psi_{ws}) \tag{3}$$

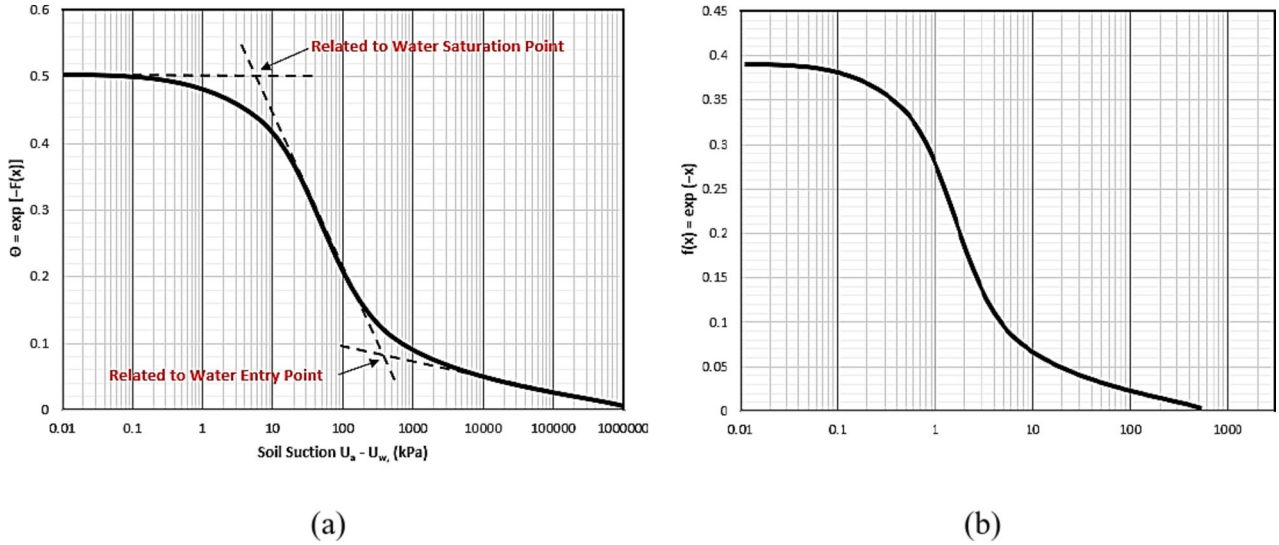

Fig. 1. (a) Typical unimodal wetting SWCC graph, (b) Graph of reciprocal of exponential function.

	Soil type	qs_1/S_e	y_{a1} (kPa)	y_{a2} (kPa)	RMSE	R^2 (%)	Source
1	Mature granite residual soil	0.412	1.1	352	0.022	99.28	Coutinho et al. (2011)[48]
2	Tropical clayey silt soil	0.414	1.1	36.6	0.007	99.62	Jotisankasa et al. (2010)[49]
3	Granite residual soil	0.32	0.25	50	0.006	99.28	Rahardjo et al. (2012)[50]
4	Hong Kong saprolite soil	0.334	1.1	13	0.012	98.41	Satyanaga et al. (2013)[39]
5	Jurong formation, residual soil	0.236	23.9	253	0.003	98.63	Rahardjo et al. (2004)[51]
6	Compacted silty sand I	0.339	6	35	0.011	99.03	Satyanaga et al. (2013)[39]
7	Pelletized diatomaceous earth	1	0.0001	46	0.018	99.43	Burger and Shackelford (2001)[20]
8	Residual, highly collapsible clay	1	5.27	17.53	0.037	98.55	Coutinho et al. (2011)[48]
9	Compacted silty sand II	1	12	30	0.002	99.55	Zhai et al. (2017)[52]
10	Compacted silty sand III	1	0.978	31.61	0.002	99.34	Zhai et al. (2017)[52]
11	Colluvial soil	0.50	3	630	0.002	96.54	Yeh et al. (2021)[53]
12	Sandstone	0.46	1.2	900	0.001	97.20	Yeh et al. (2021)[53]
13	Compacted silty sand IV	1	10	45	0.0012	99.72	Zhai et al. (2017)[52]

Table 1. Summary of bimodal soil data used in the parametric study and calibration process reproduced from Zhao, et al.[47].

$$\mathrm{F}(\psi) = \exp\left[-\mathrm{t}\left(\frac{\psi - \psi_{ws}}{\psi_{we} - \psi_{ws}}\right)\right];\ \text{when}\ (\psi) \geq (\psi_{ws}) \tag{4}$$

where, (ψ_{ws}) and (ψ_{we}) are suctions at water saturation and entry points respectively.

Zhao, et al.[47] developed a general multimodal SWCC equation in which the authors emphasized the importance of smooth connection between two adjacent sub-curves, and the continuity of the best-fitting line. A smooth transition between adjacent sub-curves is important for a number of reasons. First, theoretically, a smooth transition would provide an accurate delimiting point. A point indicating the relationship between the dominant pore sizes in dual porosity soil. Also, experimentally, the delimiting point been an important parameter in the proposed model, it helps in attaining a better fitting performance.

In the study, two important parameters (t and m) were obtained by reducing the variation between data in the published literature and measured data using the least square method. Several soils datasets (Table 1) were used to establish the value of the parameters (t and m) as *0.3* and *5.0* respectively.

Parameter (t) is an exponential decay constant, whose value determines the steepness of the curve. The value is pegged at (*5.0*) based on the parametric study by Zhao et al.[47]. In this study, upon conducting more trial of additional soil datasets, values ranging between *4.5* and *5.0* proved to offer greater fitting and better performance for this model. The two extreme values of *4.5–5.0* represent the model performance for different soils ranging from dense tropical clay to residual sand. There is then a need to adopt a value which may give mean representation for all soil types, and a value which do not temper with overall performance of the model. Hence, *4.75* is adopted.

Therefore, the equation for each sub-curve for bimodal wetting SWCC is obtained by equating the normalized water content to the reciprocal of the exponential function as shown in Eq. (5).

$$\frac{\theta - \theta_{min}}{\theta_{max} - \theta_{min}} = exp\left[-4.75\left(\frac{\psi - \psi_{ws}}{\psi_{max} - \psi_{ws}}\right)\right] \tag{5}$$

$$(\theta - \theta_{min}) = (\theta_{max} - \theta_{min})\, exp\left[-4.75\left(\frac{\psi - \psi_{ws}}{\psi_{max} - \psi_{ws}}\right)\right] \tag{6}$$

$$\theta(\psi) = \theta_{min} + (\theta_{max} - \theta_{min})\, exp\left[-4.75\left(\frac{\psi - \psi_{ws}}{\psi_{max} - \psi_{ws}}\right)\right] \tag{7}$$

A bimodal SWCC could be regarded as a combination of two sub-curves related to soil with two dominant pore sizes family (micropore and macropore series), and its equation could simply be a super-imposition of the two equations of its two sub-curves. The area of low suction is linked to the coarse macropores while the high suction area is linked to the soil's finer micropores as noted by several studies such as Durner, Rahardjo et al. and Satyanaga et al.[39,51,54].

The bimodal wetting SWCC has unique variables that define its key properties as shown in Fig. 2. First is the saturated water content of the first sub-curve (θ_{max}), which signifies a water content at which the soil macropores are fully filled with moisture. Since water first fills the soil's smallest pore, this water content indicates that the soil is fully saturated.

The other moisture contents include saturated water content of the second sub-curve (θ_{mid}), which signifies a water content at which the soil micropores are fully filled with moisture, and the minimum water corresponding to the highest recorded suction in the laboratory (θ_{min}). The other variables are water saturation points of the sub-curves 1 and sub-curve 2 (ψ_{ws1} and ψ_{ws2}) respectively, related to the suction at which the macropores and micropores are saturated, and then the water entry points (ψ_{we1} and ψ_{we2}) of the two sub-curves related to when water enters both pores.

The proposed equation to best fit the wetting bimodal SWCC is then given as;

$$\theta(\psi) = \left\{\theta_{min} + (\theta_{ws} - \theta_d)\, exp\left[-4.75\left(\frac{\psi - \psi_{ws1}}{\psi_{wd} - \psi_{ws1}}\right)\right] + (\theta_d - \theta_{min})\, exp\left[-4.75\left(\frac{\psi - \psi_{ws2}}{\psi_{max} - \psi_{ws2}}\right)\right]\right\} \tag{8}$$

where:

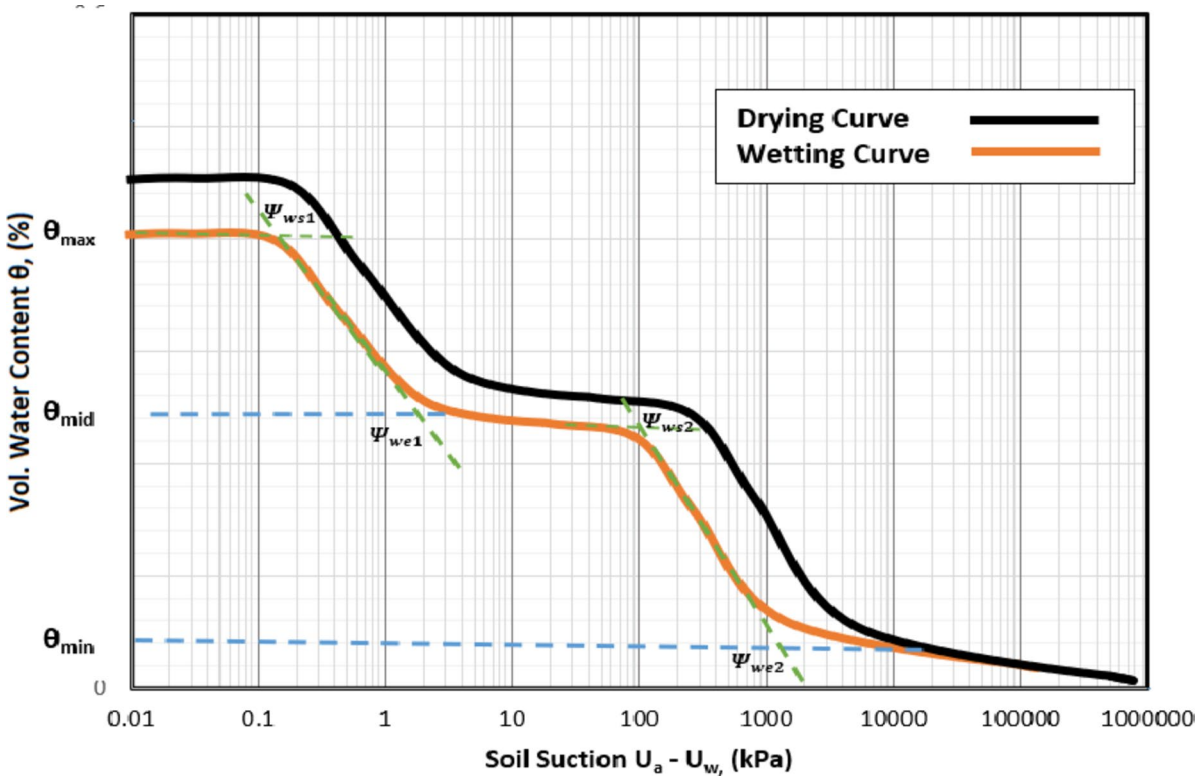

Fig. 2. Key parameters of typical wetting bimodal SWCC.

Subscripts (1) and (2) are related to the sub-curves (1) and (2) respectively representing the macropores and micropores distribution of the dual porosity soil.

θ_{ws} is the water content at saturation.

θ_{d} is the water content at the delimiting point.

θ_{min} is water content corresponding to highest laboratory recorded suction or water entry point of the sub-curve 2.

$\psi_{ws1}$and ψ_{ws1} are water saturation points related micropores and micropores of the two sub-curves respectively.

ψ_{max} is the maximum suction recorded at the laboratory.

In order to have a smooth transition between the curves, a wetting delimiting point (ψ_{wd}) that marks the ending and the beginning of the two connected sub-curves is adopted, as advocated by[39,47] "equation (9)".

$$\psi_{wd} = \psi_{ws1}^{m} * \psi_{ws2}^{1-m} \tag{9}$$

Constant (***m***) is a delimiting point parameter related to hydration - dehydration rate at the transition part where the curve is adjusting to the change from initial condition. Delimiting points in this study are determined based on wetting saturation points of the two adjacent sub-curves. The point is related to the position of the two saturation points of the two curves and controlled by the slope of the sub-curve 1. The proposed model is sensitive to the value of constant (***m***). The value of (***m***) is inversely proportional to the value of delimiting point. For example, increasing the value of the constant (***m***) above ***0.3*** causes a decrease in the value of delimiting point and thereby leading to more steepness to slope of sub-curve 1. This would push the curve to the left and significantly reduce the performance of the model. Reducing the value below ***0.3*** would shift the curve forward towards the drying curve and reduce the hysteresis loop. The value ***0.3*** is hence an ideal choice as applied to different soil types.

If the curve needs to be pushed to the entire suction range (i.e., 0 kPa – 10^6kPa), the Fredlund and Xing[2] correction factor could be applied to the equation, and then Eq. (10) would be;

$$\theta(\psi) = \left\{ \theta_{min} + (\theta_{ws} - \theta_{d}) exp\left[-4.75\left(\frac{\psi - \psi_{ws1}}{\psi_{wd} - \psi_{ws1}}\right)\right] + (\theta_{d} - \theta_{min}) exp\left[-4.75\left(\frac{\psi - \psi_{ws2}}{\psi_{max} - \psi_{ws2}}\right)\right] \right\} \left[1 - \frac{In\left(1 + \frac{\psi}{\psi_{we2}}\right)}{In\left(1 + \frac{10^6}{\psi_{we2}}\right)}\right] \tag{10}$$

ψ_{we2} is the water entry point of sub-curve 2, indicating the suction when water first enters the smallest pore of the soil.

The proposed equation constitutes parameters with relative physical meaning with the known variables of bimodal wetting SWCC. For example, these parameters represent properties in relation to moisture movement in soil pores. A brief description of such mechanisms is as follows.

a. Wetting Saturation Point 1 (ψ_{ws1}): This first suction value at which all the soil pores are completely filled with water and all air are expelled.
b. Wetting Saturation Point 2 (ψ_{ws2}): This suction value at which all the soil micropores are completely filled with water, and moisture begins to fill the macropores.
c. The Delimiting Point (ψ_{wd}): This is the suction value marking the end and the beginning of two successive curves for soil with dual porosity. It physically relates to the demarcation between the two dominant pore-size distribution of a dual-porosity soil.
d. Water Entry Point 2 (ψ_{we2}): This is suction value which breaks through the interface between air and water (contractile skin) and begin wetting the smallest pore in the soil.
e. Moisture Contents: The three moisture contents namely, saturated water content (θ_{ws}), delimiting water content (θ_{d}) and minimum water content (θ_{min}) are related water contents at saturation point, delimiting point and the water entry point respectively.

It is worth noting that, if the laboratory dataset indicates a unimodal SWCC, the same equation could in part be applied to best fit the unimodal wetting SWCC. This is by using the first sub-curve part of Eq. (10) and substituting the wetting delimiting point (ψ_{wd}) with the water entry point of sub-curve 1 (ψ_{we1}).

Evaluation criteria

To evaluate the performance of the proposed equation, data of bimodal wetting SWCCs is needed. Moreover, the availability of such data in the literature is very scarce. This is related to the difficulties of conducting wetting SWCC test in the laboratory. Meanwhile, five datasets, from literature in Liu, et al.[55] and Najdi, et al.[56], which are named soils S1, S2, S3, S4 and S5, are obtained and used. In order to satisfy the validity of the proposed model for a wider range of soil types, six other hysteretic tests of soils with wide ranges of properties are conducted (S6, S7, S8, S9, S10 and S11) are used as well, to examine the validity of the proposed equation. The rate of the model performance is measured using statistical methods. The eleven wetting bimodal datasets are best fitted with the proposed developed equation [Eq. 8)]. Its performance is evaluated using root mean square error (RMSE) and coefficient of determination (R^2).

First the initial (assumed) curve's parameters are obtained graphically from the laboratory data points, then an iterative non-linear regression procedure is used to adjust and best fit all parameters. Since all the parameters

of the proposed equation have physical meaning, all the variables of the SWCC could simply be read from the best-fitting data.

Soils properties and methods used in the study

Due to difficulty associated with performing wetting SWCC in laboratory, the availability of wetting bimodal SWCC data is very rare in the literature, and a comprehensive search of such data returned a very scant result. However, some natural soils data having complete hysteretic bimodal SWCC are found in the literature and used. The choice of the samples is based on soil having both bimodal drying and wetting curves, completeness of the data and the range of the suction. A granite residual soil (S1 and S2) from Guangdong China in Liu, et al.[55] and a low-plasticity clayey soil (S3, S4 and S5) from Agropolis, Barcelona in Spain in Najdi, et al.[56] both found in the literature were used. An additional six other hysteretic tests of soils with wide ranges of properties are conducted (S6, S7, S8, S9, S10 and S11), and used in evaluating the performance of the proposed equation using laboratory engineered soil. The published data were obtained from the plots of the publications of the SWCCs in both Liu, et al.[55] and Najdi, et al.[56]. The soil samples used in this study, provide a wider range of representations, covering a good range of soil types from "silty sand to low plasticity clay". Two important soil properties that dictate the shape and often modality of SWCC are moisture content and dry density. The soil samples used in this work to validate the proposed equation covered a wide range of those properties. The eleven samples, as shown in Table 2, are between 6.7 and 22% moisture content ranges, while the dry densities span between 1.30 g/cm^3 to 1.89 g/cm^3.

The engineered soil samples chosen for this study is made up of silty sand as popularly used due to its homogeneity and an "inert" coarse kaolin, which according to Satyanaga, et al.[57–59], do not yield an excessive volume change due to heat exposure.

Prior researchers such as Satyanaga, et al.[39] and Zhao, et al.[47] shows that a mix of sand and kaolin at certain proportions and compacted at the dry of optimum, yields a soil sample that produce a bimodal SWCC. This study follows this same procedure. Data of the soils S1, S2, S3, S4 and S5, were adopted from the literature in Najdi et al. 2023 and Liu et al. 2023. Additional soil compositions (S6, S7, S8, S9, S10 and S11) made up of 80% sand and 20% kaolin, 70% sand and 30% kaolin, 60% sand and 40% kaolin, 40% sand and 60% kaolin, 30% sand and 70% kaolin, and 20% sand and 80% kaolin respectively were used in this study.

First, a non-uniform, brown granite residual soil obtained from Guangdong China is crushed after been dried at room temperature and then screened through a 2 mm sieve. The soil shows a composition of mainly sand, silt, and a little amount of clay from the results of grain size distribution. A light compaction test was conducted on the soil to ascertain its optimum moisture content and the corresponding maximum dry density. The soil is then sub-divided into different samples (S1 and S2) and categorized by varying water contents and dry densities in order to study its hysteresis characteristics.

Samples S3, S4 and S5 were prepared using Agropolis clay having low plasticity, obtained from Barcelona, Spain. The basic properties of the clay material are as shown in Table 2, the samples are prepared by varying the soil's initial moisture content. Their optimum moisture contents and maximum dry densities were obtained from which the SWCC samples were prepared. The tests were conducted combining multiple methods of Northumbria High Capacity Tensiometer (N-HCT) and Dewpoint Potentiometer (WP4C).

Index properties test

In this study, index properties of the soils (S6 - S11) were obtained based on procedures described in American Society for Testing and Materials (ASTM) standards as follows; Soil Classifications are based on Unified Soil

Soil Name	S1	S2	S3	S4	S5	S6	S7	S8	S9	S10	S11
Soil Type	Residual Granite Silty Sand	Residual Granite Silty Sand	Low-Plasticity clay	Low-Plasticity clay	Low-Plasticity clay	Engineered Soil from laboratory testing in this study	Engineered Soil from laboratory testing in this study	Engineered Soil from laboratory testing in this study	Engineered Soil from laboratory testing in this study	Engineered Soil from laboratory testing in this study	Engineered Soil from laboratory testing in this study
USCS	SM	SM	CL	CL	CL	MI	MI	CL	CL	SM	SM
Sand (%)	50.1	50.1	48.3	48.3	48.3	20.0	30.0	40.0	60.0	70.0	80.0
Silt (%)	46.8	46.8	42.1	42.1	42.1	76.0	66.5	57.0	38.0	28.5	19.0
Clay (%)	3.1	3.1	9.6	9.6	9.6	4.0	3.5	3.0	2.0	2.5	1.0
OMC (%)	20	20	16	16	16	17.8	14.7	12.0	10.5	10.1	10.0
MDD (g/cm^3)	1.69	1.69	1.76	1.76	1.76	1.69	1.77	1.83	1.93	1.94	1.95
Liquid Limit	39.4	39.4	29	29	29	38.0	34.0	27.5	23.0	20.0	19.3
Plastic Limit	23.9	23.9	17	17	17	22.1	19.1	17.2	13.4	12.5	11.8
Plasticity Index	15.5	15.5	12	12	12	15.9	14.9	10.3	9.6	7.5	7.5
Specific Gravity	2.54	2.54	2.70	2.70	2.70	2.55	2.56	2.60	2.61	2.63	2.64
Initial Moisture Content (%)	14	22	17	21	15	17.1	14.2	11.64	10.19	6.9	6.7
Initial Dry Density (g/cm^3)	1.30	1.70	1.78	1.72	1.89	1.68	1.76	1.82	1.83	1.88	1.89

Table 2. Index properties of the soils used in validating the proposed equation.

Classification System (USCS) covered by ASTM-D2487-17[60], Grain Size Distribution according to ASTM-D6913M-17[61]. Atterberg Limits according to ASTM-D4318-17[62]and the Specific Gravity as covered by ASTM-D854-14[63]. The Standard Proctor Compaction test is based on ASTM-D698-12[64] to ascertain the soil's Optimum Moisture Content and its corresponding Maximum Dry Density. Thus, 97% of maximum dry density at the dry side of optimum was chosen for SWCC samples preparations.

SWCC tests

Matric suction is a state variable causes by soil particles capillarity on pore-water[65]. Several techniques are available to measure matric suction directly or indirectly. In indirect measurements such as using gypsum block, thermocouple psychrometers and soil moisture sensors (e.g. TDR or FDR sensors), calibration is needed to link the relationship between the property of the measured particles and the matric suction. This enables the matric suction to be measured through relating the value of the measured property and the calibration curve. But this method leads to some form of low accuracy in the suction measurement compared to direct methods. This is due to the difference of properties between the suction and the measured property[66].

To solve this problem, direct methods such as polymer sensors are used, in this method, suction is measured in relation to a drop in pressure between the water chamber in the sensor and the surrounding soil. Matric suction is measured when an equilibrium is attained between the two[67]. For this reason, several tensiometers (such as water filled tensiometer) using the same principle are being used to measure the suction directly. But still, these types of tensiometers are limited with a problem of cavitation, due to the presence of undissolved air nuclei. This is in the form of entrapped air which often gathers and appears at the corner of the reservoir. This prevents measurement of soil suction above 100 kPa. High suction polymer sensors (HSPS) are the newly developed polymer-based sensors made primarily to solve the cavitation problem. Polymer sensors have some features that differentiate it from other forms of sensors. Allowing it to be the best alternative compared to the conventional sensors available, particularly in terms of elastic, mechanical, chemical, and electro-kinetic characteristics.

Generally, this type of tensiometer is composed of 3 separate components: pressure transducer, water chamber and ceramic disk. When the sensor is lowered on the soil sample and the disk comes into contact with the unsaturated soil sample, water in the middle chamber flows down through the ceramic disc into the surrounding soil. This contact and the resulting water flow thus create a tension state within the water chamber, and this is sensed and read by the pressure transducer. The transducer will then signal the pressure change to the computer where all the records are made and kept. This keeps going until the equalization of pressure between the chamber and the surrounding soil is reached, which is indicated as constant successive reading on the screen. At this point, the suction could be noted as the difference between the initial pressure (at sample saturation) and the current pressure reading. Pictorial description of HSPS is shown in Fig. 3. Although the HSPS provides a

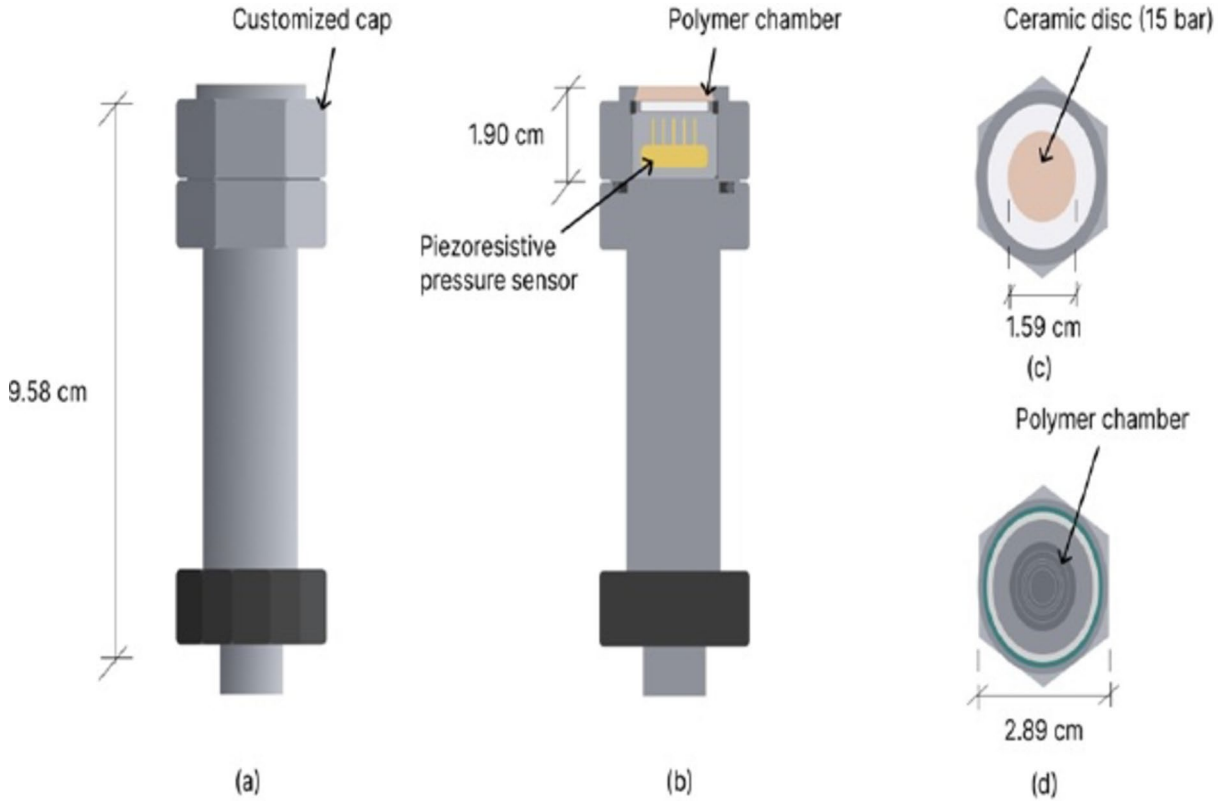

Fig. 3. Schematic diagram of High Suction Polymer Sensor (HSPS).

good opportunity to measure suctions above 100 kPa, it is only utilized in drying SWCC measurement and there is no report of it been used in measurement of wetting SWCC. This work measured both the drying and wetting SWCC at the suction of 0 kPa – 1500 kPa using the High Suction Polymer Sensor [Fig. 3].

The HSPS used in this study is developed using a synthesized polyacrylamide (PAM), with a varying degree of cross-linking using ultraviolent polymerization[67]. These specific PAM based tensiometers have better stress relaxation than NaPA (sodium polyacrylate) based. It has better attribute of maintaining constant pressure for a long period without the need for correction due to pressure decay rate. However, with measuring range of highest accuracy between 10 kPa – 1500 kPa, PAM-filled tensiometers measuring range is lower than that of NaPA-filled tensiometers[68]. The calibration of the sensors before each round of measurement involves saturating it in de-aired water to enable the polymer to attain the highest swelling and then the corresponding highest pressure recorded to be used in calculating the suction at each stage of the on-going test.

The SWCC test on the soil samples (S6 - S11) was done by combining measurements from two different equipment, first by measuring the low suction (0 kPa – 1500 kPa) using a high suction polymer sensor (HSPS) based on similar procedures followed Liu, et al.[67] and Liu, et al.[68], and the high suction (1500 kPa – around 300 MPa) using a dewpoint potentiometer (WP4C) as described by Leong, et al.[69]. The wetting curve is then fitted using the proposed equation [(Eq. 8)] developed in this study. The choice of using high suction polymer sensor is to enable faster determination of the SWCC at low suction value as compared to the usual use of Tempe Cell. Moreover, as WP4C usually measures suction with accuracy (to within 50 kPa) only from about 1000 kPa and above, combining HSPS with WP4C closes the gap (100 kPa – 1000 kPa) usually encountered in using the combination of Tempe Cell and WP4C.

Drying SWCC

Before the drying SWCC test begins, the sample is prepared based on ASTM D6836-16. The soil specimen is compacted at the 97% dry of optimum into 80 mm in diameter and 20 mm in height, in a mold (specifically fabricated for this study and shown in (Fig. 4) and placed onto the water bowl for saturation. The kaolin used is a silty clay that doesn't undergo significant volume change even at high percentage as compared to initially tested bentonite as identified in this study and similarly noted by Hatefi et al.[70]. So, volume change intricacies are not considered in this work. The sample is weighed periodically until the mass becomes constant, confirming its total saturation. To enhance the chance of achieving a bimodal SWCC, past studies on dual porosity soils such Satyanaga, et al.[39] and Zhao, et al.[47] usually compacts the soil compositions at 95% dry of optimum. However, in this study, 95% is considered too dry to generate good and quality soil sample, therefore, 97% wet of optimum was selected. The drying SWCC measurement using the High Suction Polymer Sensor (HSPS) was then begun by placing the sensor on a small groove of 5 mm depth and diameter equals to the sensor bulb, made at the center of the sample. The sensor was then placed vertically upright and with its bottom tip completely covered in the sample. This is to avoid having any cavity or partial contact between the soil and the sensor, which can cause a significant data fluctuation. The whole setup is then placed on a weighing scale with the sensor connected to a computer system for the continues measurement of the suction. The weighing scale used is equally of very high accuracy to enable measurement of smallest moisture change, as this is very crucial in computing the overall water content variations. It measures the soil suction as a response to water pressure drop in the chamber when

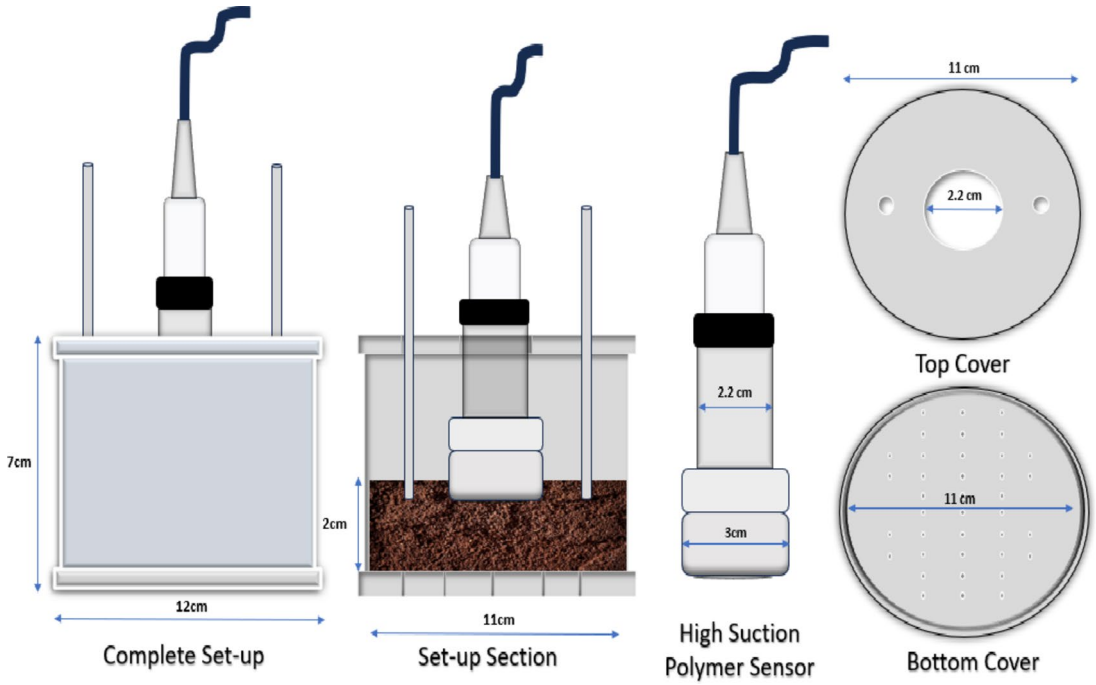

Fig. 4. Complete set-up for novel wetting SWCC using high suction polymer sensor (HSPS).

the ceramic disk is in direct contact with an unsaturated soil, and the water flows out through it, which will equalize (be in equilibrium) gradually over time (Liu et al. 2023). The top of the sample is left exposed and allows the sample to dry for usually 1–3 h (depending on the soil's moisture content) under room temperature. The sample is then covered to allow total moisture equalization within the sample, the equalization is indicated when the pressure reading becomes constant for at least 3 consecutive readings or reaches its peak and began to drop, and then the current pressure and weight are noted. This cycle is repeated several times to obtain enough data for the low suction range. Usually, measurement with the sensor will be stopped when the suction reading reached around 1500 kPa. The WP4C dewpoint potentiometer works by measuring the relative humidity on the soil surface within a small chamber in the equipment, using the chilled-mirror dewpoint technique. The suction and the sample temperature are directly displayed on a screen. The measurement of high suction using WP4C is conducted by first preparing a sample at the required density in a standard WP4C mold. The sample is periodically dried outside the chamber and allowed to cool with its mass both before and after the drying is noted and then placed back into the chamber for suction measurement. This cycle continues until the highest suction measurement of usually around 300 MPa is achieved.

Wetting SWCC

For the measurement of wetting SWCC using high suction polymer sensor, the mold containing the sample is first covered with a special lid with a hole of 22 mm at the center equals to the diameter of the sensor's stem [(Fig. 4)]. This central hole is sandwiched between two other holes of 2 mm each from which tubes are inserted to enable periodic wetting of the soil sample as the test is ongoing. It is imperative that the soil sample is sealed throughout the test period to avoid loss of moisture from the sample due to evaporation.

The test process consists of replenishing the soil moisture periodically through the tubes using a syringe, while the sensor measures the change in suction. The tubes used for wetting the sample are located midway between the sensor and the mold perimeter. This is to avoid having inaccurate results that may be caused by over-wetting the sample near its center, while its side remains dry.

The equalization between the water inside the sensor and the surrounding soil is indicated by having a negligible suction change or by 3 to 4 consecutive constant suction reading below 0.3 kPa. Only then water would be added, and the same cycle is repeated until the full saturation of the sample is re-achieved.

For the high suction measurement of wetting SWCC using WP4C potentiometer, the wetting is started upon completion of the drying test. The process consists of adding drips of distilled and de-aired water on the prepared and oven dried soil samples in the WP4C mold and measuring the new mass for moisture content measurement.

The samples are allowed to cool and then inserted into the WP4C chamber one after another for suction measurements, until enough drips are made to record the low suction of around 1500 kPa.

The two results of both water content and suction from the high suction polymer sensor and the WP4C potentiometer are combined and fitted using the proposed equation [Eq. (8)] to obtain the wetting SWCC.

Results and discussions

Index properties

Sand and kaolin were mixed in six different compositions. This is to obtain engineered dual porosity soils covering wider range of properties and yielding a bimodal SWCC, as obtained in similar other studies such as in[16,39,47,71]. Various index properties tests were conducted on the soil samples and the results are summarized in Table 2. All the samples exhibit bimodal SWCC. Table 2 gives the results of basic index properties of all the soils used in validating the proposed equation.

Results of particle size distributions and standard proctor compaction tests for the laboratory engineered soils used in this study, and other soil from literature are presented in Figs. 5, 6 and 7.

Figure 5 have shown that all the 6 engineered soils used are gap-graded which is characterized by dual porosity. Equally, Fig. 6 has shown that for all the soils used, with the increase in sand content, there is an increase in dry density and decreases in moisture content. This is typical for soil with bigger particles such as sand. Likewise, the increase in water content with an increase in kaolin content is related to the clay soil moisture retention ability.

SWCC test

A combination of two methods using High Suction Polymer Sensor (HSPS) and Dewpoint Potentiometer (WP4C) were used to obtain both drying and wetting SWCC data for this study. The relevant wetting bimodal SWCC variables obtained from the tests are summarized in Table 3. Both drying and the wetting curves for soils samples with lower fine content in this study show a wider hysteresis loop in the low suction zone (macropore range). This is caused by the effect of entrapped air. This is evidently shown in the results through the difference between saturated volumetric water content between the drying and the wetting curve by about 10% as noted by Pham, et al.[16], and is in agreement with various studies such as Satyanaga et al. (2013) and Zhai, et al.[72]. Past studies on hysteresis of SWCC such as in Kristo and Rahardjo[9] and Satyanaga, et al.[13] did not measure wetting SWCC in high suction area, usually the studies always halt the measurements at or below 1500 kPa, albeit most of them are for unimodal SWCC. This study of wetting bimodal SWCC provides a chance to extend the measurement to the high suction.

It could be noted from all the results of soils in this study that the hysteresis loop is not as wide in the high suction area as compared to the low suction area. This is due to the combination of less effect of entrapped air which occurs more in macropores than in micropores, and other factors such as migration of the finer particles into macropores during wetting (particles re-arrangement), which in turn limits the amount of water the pores could absorb.

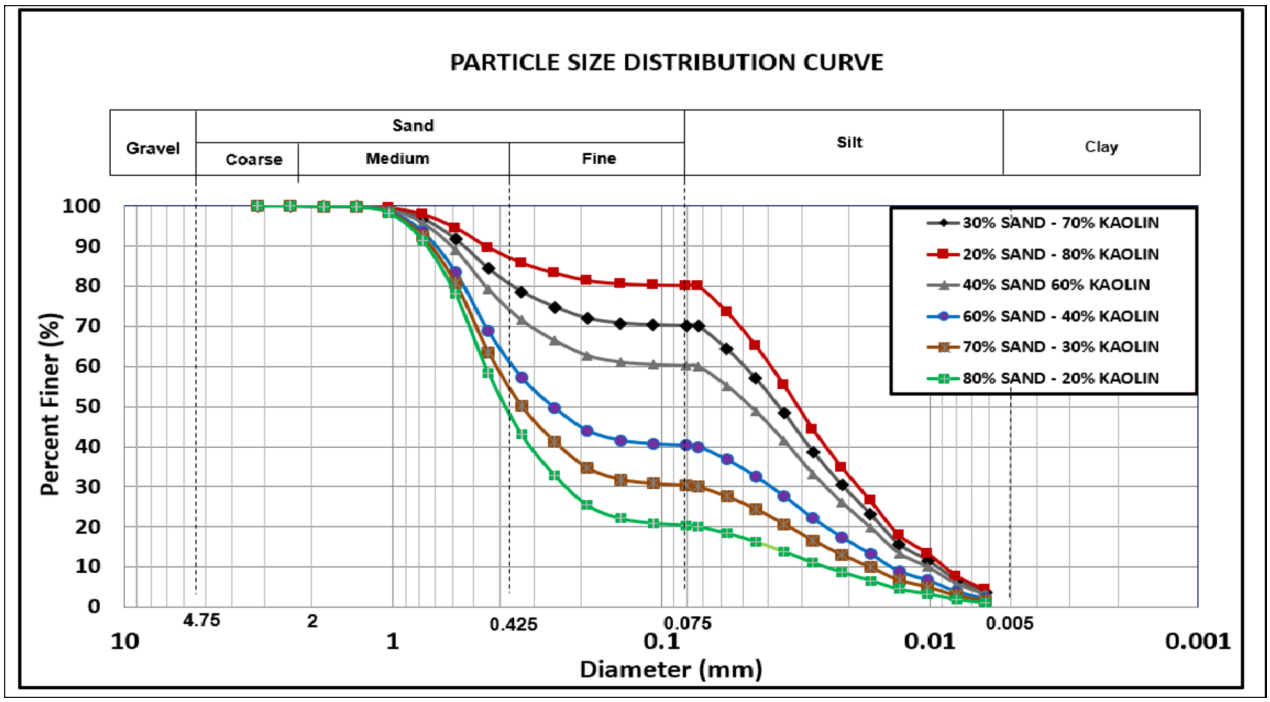

Fig. 5. Grain Size Curves for Laboratory Engineered Soils used in this study.

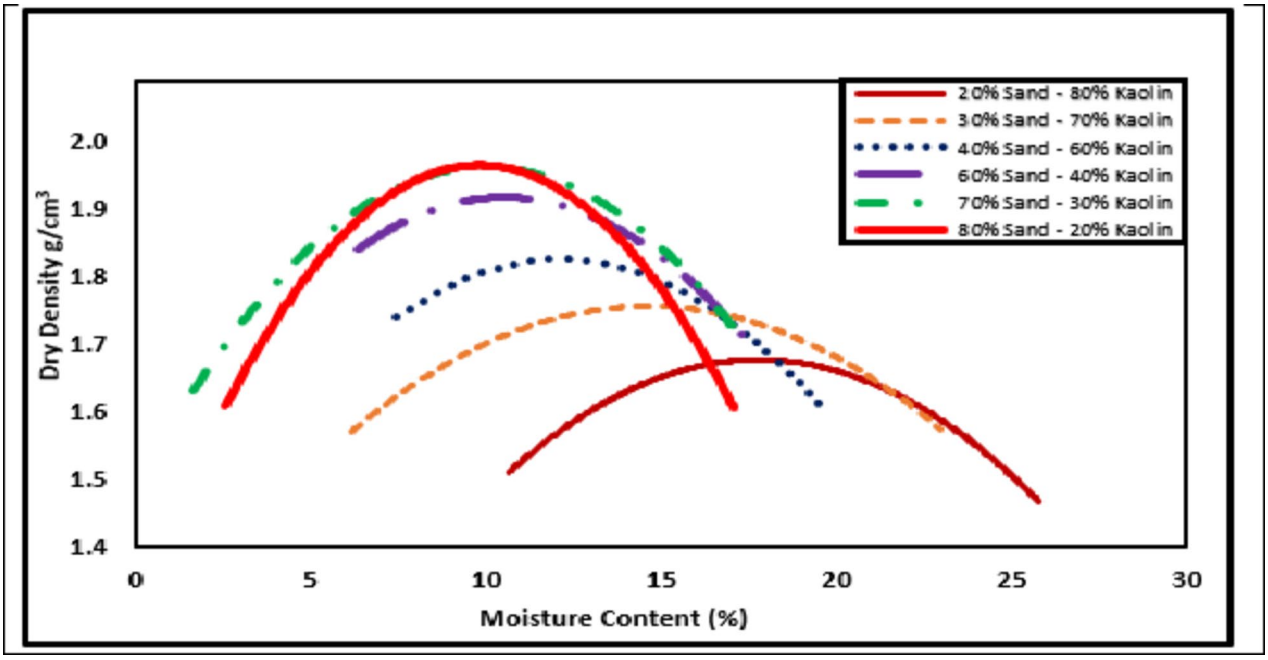

Fig. 6. Standard Proctor Compaction Curves for Laboratory Engineered Soils used in this study.

Performance of the proposed equation as compared to SWCC from laboratory data

The performance of the proposed equation as shown in Table 3is measured using co-efficient of determination (R^2) and root mean square error (RMSE) as commonly used in various similar studies such as Satyanaga, et al.[39] and Yeh, et al.[73]. The wetting bimodal SWCC equation parameters were first graphically obtained based on the shape of the SWCC from the laboratory data points or from the relevant fitting parameters from the published data. The data are then key-in to the statistical analysis software for best fitting, this is to compare the values obtained directly from the curve with the fitting values from this equation as shown in Table 3.

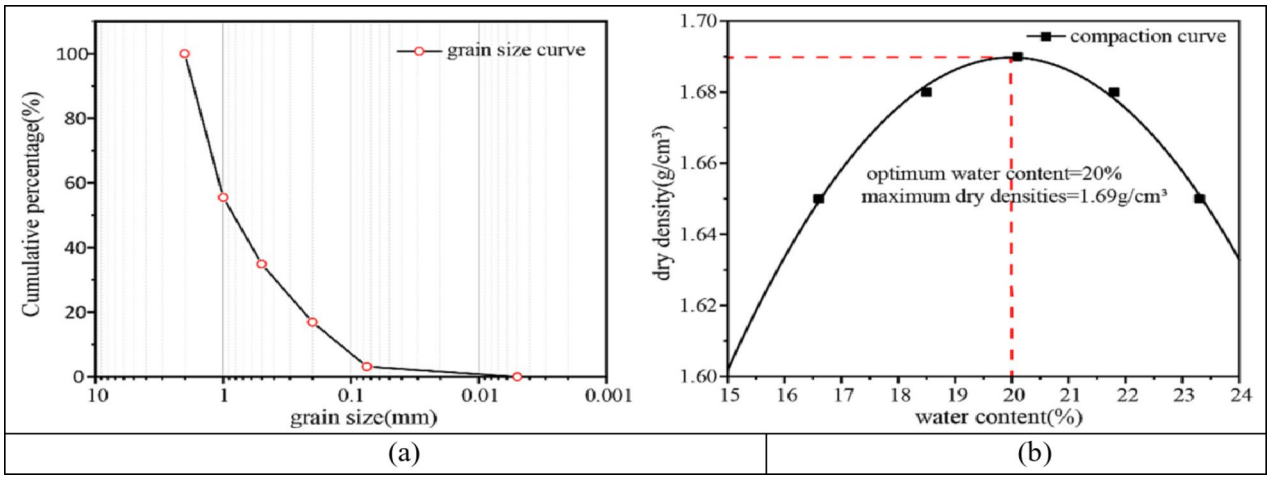

Fig. 7. (a) Grain Size Curve (b) Compaction Curve for Soils S1 and S2 (Liu, et al.[55]).

Soil type	Soil Name	Source	ψ_{ws1}(kPa)	ψ_{ws2}(kPa)	ψ_{we2} (kPa)	θ_{max}	θ_{mid}	θ_{min}	RMSE	R^2
Granite Residual 1	S1	Liu, et al[55].	4.70	314.64	310.85	24.16	18.38	8.81	0.007	0.999
Granite Residual 2	S2	Liu, et al[55].	4.67	276.09	312.57	24.14	18.36	5.25	0.007	0.999
Low-Plasticity clay 1	S3	Najdi, et al[56].	71.78	215.75	1250.09	0.87	0.78	0.58	0.014	0.999
Low-Plasticity clay 2	S4	Najdi, et al[56].	50.61	195.42	271.51	0.91	0.83	0.68	0.005	0.999
Low-Plasticity clay 3	S5	Najdi, et al[56].	0.29	1501.11	1371.7	0.78	0.56	0.41	0.008	0.999
20% Sand – 80% Kaolin	S6	Laboratory testing in this study	30.16	220.52	29.6	0.566	0.420	0.12	0.0009	0.996
30% Sand – 70% Kaolin	S7	Laboratory testing in this study	4.95	127.63	48.8	0.468	0.411	0.176	0.0004	0.998
40% Sand – 60% Kaolin	S8	Laboratory testing in this study	4.7	41.5	60.4	0.413	0.318	0.139	0.0070	0.999
60% Sand – 40% Kaolin	S9	Laboratory testing in this study	4.64	17.00	3577.0	0.286	0.189	0.046	0.0005	0.998
70% Sand – 30% Kaolin	S10	Laboratory testing in this study	4.01	136.4	15.3	0.234	0.170	0.095	0.0001	0.999
80% Sand – 20% Kaolin	S11	Laboratory testing in this study	3.99	137.00	5500	0.177	0.103	0.031	0.0001	0.995

Table 3. Best fitting parameters for evaluating the performance of the proposed equation.

There are total of eleven (11) sets of bimodal datasets (S1 – S11) used in validating the equation and to gauge its performance. These datasets as presented in Table 2, represents a wide range of initial moisture content (6.7 – 22%) and initial dry densities (1.30 g/cm^3 – 1.89 g/cm^3), which together influences the SWCC bimodality of a soil sample. For soil S1 (Fig. 8a), the R^2 and RMSE are 0.9993 and 0.007 respectively, and the proposed equation fits very well with the wetting bimodal SWCC data points, showing a good performance. The first and the second water saturation points of the proposed equation (ψ_{ws1} and ψ_{ws2}) are 4.70 kPa, and 314.64 kPa respectively, which correspond well with the same SWCC parameters of the published data in[55].

For the soil S2 (Fig. 8b), the R^2 and RMSE are also 0.9992 and 0.007, respectively. The first and second water saturation points from the proposed equation (ψ_{ws1} and ψ_{ws2}) are 4.67 kPa and 276.09 kPa, respectively. The second water entry point (ψ_{we2}) which signifies the suction at which water first enters into the smallest soil pore of the soil is 312.57 kPa, and all agree with the published data. Similarly, both the saturated volumetric water content of the two sub-curves in soils S1 and S2, are in agreement with the published data. Although the minimum moisture content (θ_{min}) in both cases always appears to be a little higher than the actual minimum moisture content from the experimental data, the difference is negligible to cause any significant variation. This is common in various best-fitting equations of bimodal SWCC, as equally noticed in past studies such as Satyanaga et al.[39] and Zhao, et al.[47].

The proposed equation also fitted very well with the data for soil S1 and S2 as shown in Fig. 8a and b, so is also for soils S3, S4 and S5 which were prepared using the same soil but at different initial moisture contents and dry densities as shown in Figs. 9a and b and 10. The performance evaluation of the proposed equation gives, the R^2 and RMSE of 0.9986, 0.9998, 0.9988 and 0.014, 0.005, 0.008 respectively.

This trend is equally the same for soils S6, S7, S8, S9, S10 and S11 on which tests on this study were conducted. The equation fits very well with the curves obtained from the laboratory discrete datapoints. The R^2 and RMSE of all the soils S6, S7, S8, S9, S10 and S11 are 0.996 and 0.0009, 0.998 and 0.0004, 0.999 and 0.0070, 0.998 and 0.0005, 0.999 and 0.00001 and 0.995 and 0.00001 respectively, indicating that they are all above the R^2 of 99% and with RMSE close to zero. The parameters of the equation are also quite close to the variables of the relevant SWCCs of the samples, which also indicates a good performance of the proposed equation.

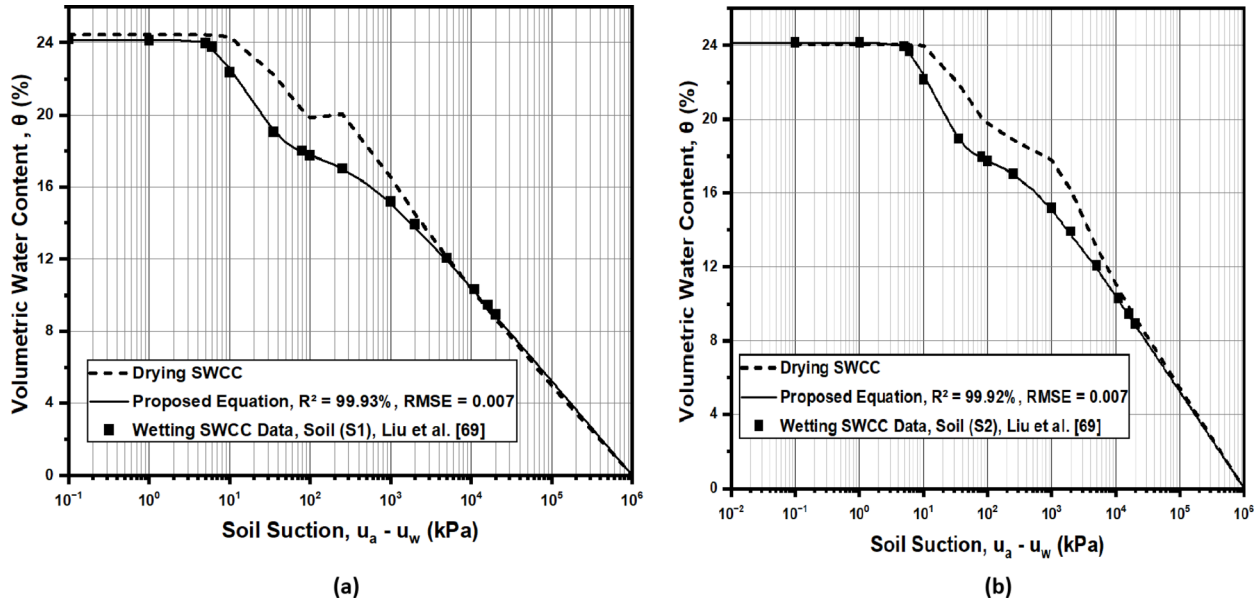

Fig. 8. Comparison between published data and the predicted SWCC of (a) soil S1, and (b) Soil S2.

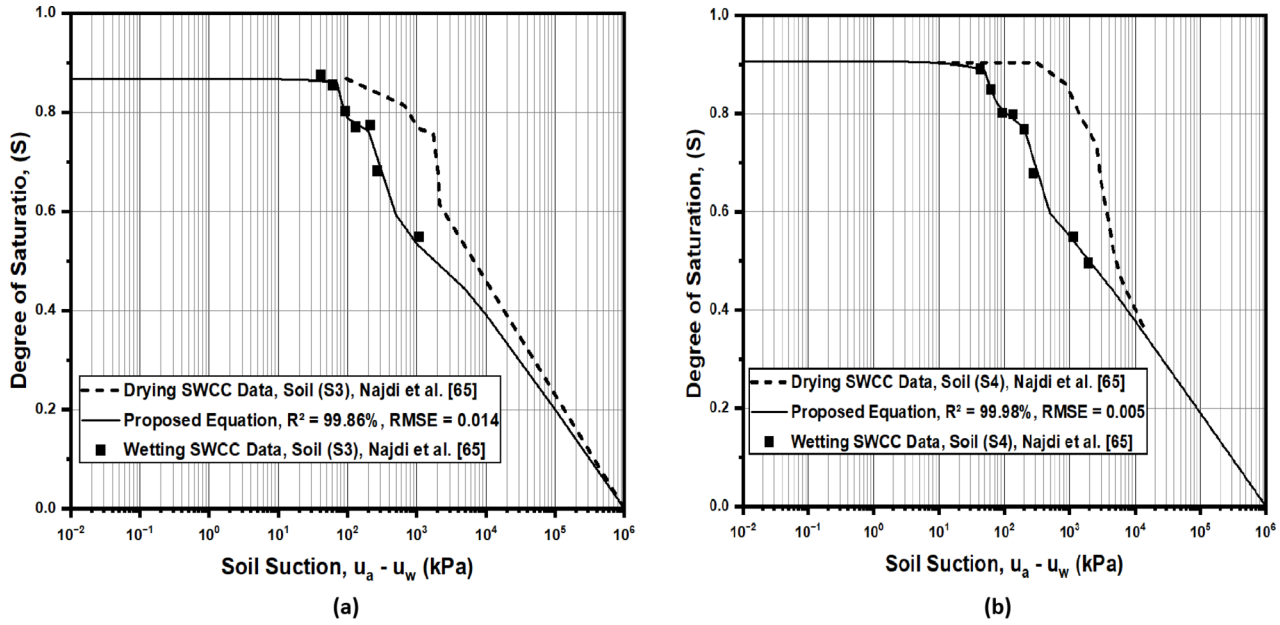

Fig. 9. Comparison between published data and the predicted SWCC of (a) soil S3, and (b) Soil S4.

Performance of the proposed equation as compared to existing model

As described in the review part, several mathematical equations to model SWCC exist. Apart from their difference in derivation method, or categories as been empirical or physically based, these models are categorized based on type of SWCC they modelled. Ideally, unimodal equations have popularly been used in the past. These unimodal equations were superimposed after recent studies recognized the bimodality of several SWCCs from dual porosity soils. The equations are then used to model bimodal SWCC. Superimposing two unimodal equations becomes a popular method, representing a sound approach, this same approach is used in this study.

Gardner (1958) equation[74] "equation (11)" is one of the earliest classical models uses by many researchers to model SWCC. The model is being used due to its simplicity and small number of parameters. A performance comparison of best-fitting ability is made between the proposed model from this study and Gardner (1958)[74]. The choice of comparison with Gardner (1958)[74] is due to its several similarities with the proposed model in terms of simplicity, method of derivation and small number of parameters.

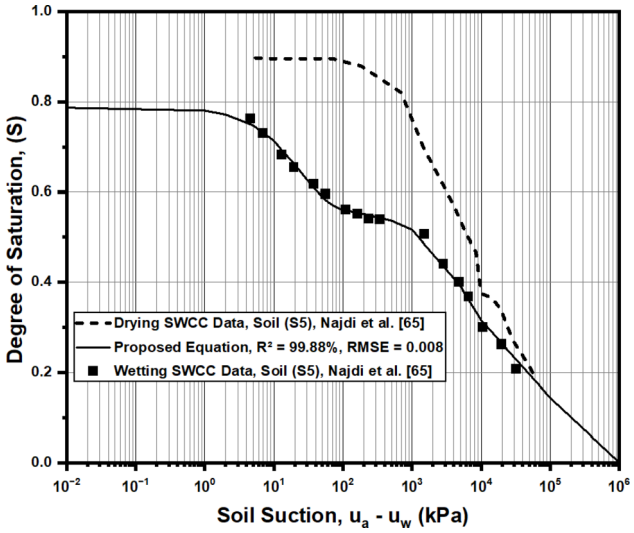

Fig. 10. Comparison between published data and the predicted SWCC of soil S5.

Model		Gardner (1958)[74]					Proposed Model			
Soil type	Soil Name	a_1	n_1	a_2	n_2	RMSE	ψ_{ws1} (kPa)	ψ_{ws2} (kPa)	ψ_{we2} (kPa)	RMSE
Granite Residual 1	S1	0.0003	0.7694	0.3200	1.0000	0.6579	4.70	314.64	310.85	0.007
Granite Residual 2	S2	0.2787	0.2618	1.5513	8.9287	0.4383	4.67	276.09	312.57	0.007
Low-Plasticity clay 1	S3	1.3E-6	1.7539	1.4823	1.6734	0.1472	71.78	215.75	1250.09	0.014
Low-Plasticity clay 2	S4	0.0817	0.3612	1.0340	0.2043	0.1629	50.61	195.42	271.51	0.005
Low-Plasticity clay 3	S5	0.0011	0.7075	0.5309	0.8939	0.1395	0.29	1501.11	1371.7	0.008
20% Sand – 80% Kaolin	S6	0.0690	0.4880	1.2529	0.4391	0.0218	30.16	220.52	29.6	0.0009
30% Sand – 70% Kaolin	S7	0.0010	1.0404	7.63E-5	4.4856	0.0037	4.95	127.63	48.8	0.0004
40% Sand – 60% Kaolin	S8	0.090	0.6205	0.7919	0.5550	0.0077	4.7	41.5	60.4	0.0070
60% Sand – 40% Kaolin	S9	0.0472	0.4936	0.8229	0.9369	0.0112	4.64	17.00	3577.0	0.0005
70% Sand – 30% Kaolin	S10	0.0868	0.5984	5.0178	15.2550	0.0054	4.01	136.4	15.3	0.0001
80% Sand – 20% Kaolin	S11	0.0009	1.0735	0.0015	3.3340	0.0027	3.99	137.00	5500	0.0001

Table 4. Comparison of fitting parameters and performance between Gardner (1958)[74] and proposed model.

$$\theta\ (\psi\ ) = \theta_{\ r} + \left[(\theta_{\ s1} - \theta_{\ s2})\left(\frac{1}{1 + a_1\psi^{\ n_1}}\right)\right] + \left[(\theta_{\ s2} - \theta_{\ s3})\left(\frac{1}{1 + a_2\psi^{\ n_2}}\right)\right] \tag{11}$$

Table 4shows a comparison between the proposed model and the Gardner (1958) model[74]for all the 11 soils used in this study. It could be noted that while the Gardner (1958)[74] present fitting parameters (a_1, n_1, a_2 and n_2) with no physical meaning in relation to variables of wetting SWCC, all the parameters from the proposed model have physical meaning. The RMSE used to assess the model performance gave more promising results with the proposed model than with Gardner (1958) equation. All the RMSE values using the proposed model are very close to zero, with an average of the 11 soils used in the validation as 0.0045. While the Gardner (1958) model gave an average RMSE of 0.1453 (Figs. 11, 12, 13).

Figures 14, 15, 16 shows the graphical comparison between the proposed model and the Gardner (1958) model. Although the Gardner (1958) model perform fairly well and fit most of the data points from the laboratory tests result, some inconsistencies could be identified. The model, similar to most of the earliest fitting models, their performance is usually low in steep slopes as shown in Figs. 14a and 15a. Another weakness is that although the model is superimposed to model bimodal SWCC, most at times its curves appear unimodal as shown in Figs. 14a, 15a and 16a. It is equally shown (based on this comparison) that the Gardner (1958)[74] model is more accurate in high suction area than in the low suction area, while the proposed model performs better throughout the SWCC range.

In general, the proposed equation provided a significant performance when tested with all the eleven datasets. All the R^2 are greater than 99%, with an average of eleven datasets at 0.998 and the RMSEs are very small and approaching (0), with an average of 0.005. Another important attribute of the equation is that, not only volumetric water content (θ), could be used, depending on the data available, either gravimetric (w_g) or

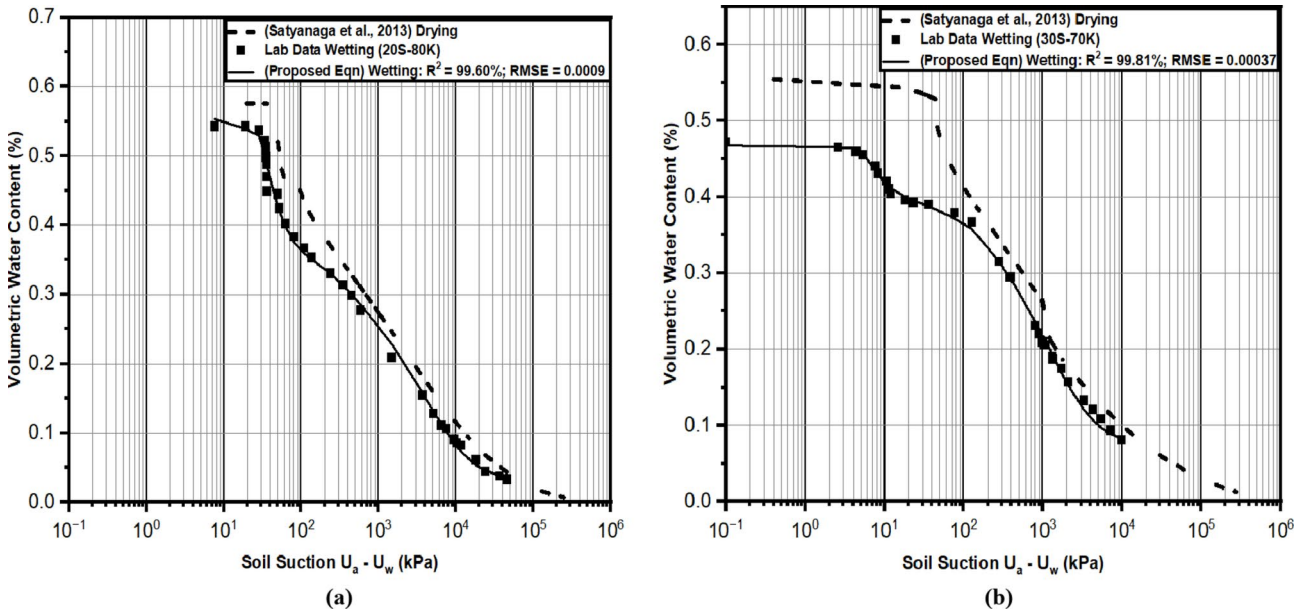

Fig. 11. Comparison between predicted SWCC and results from this study (a) soil S6, and (b) soil S7.

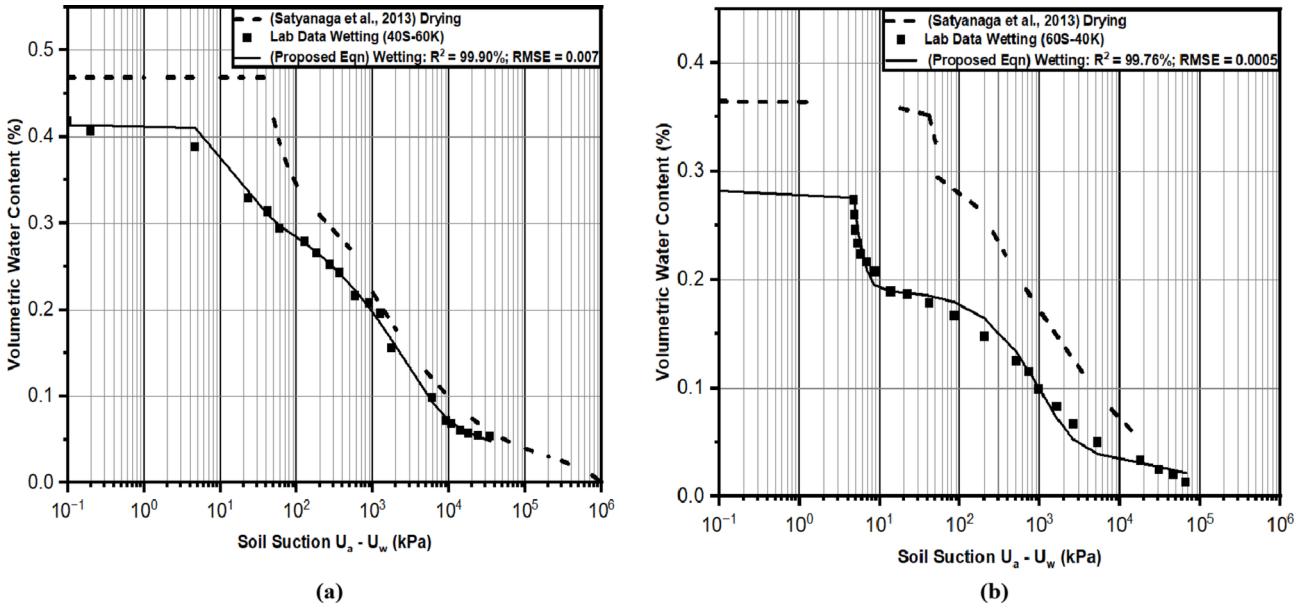

Fig. 12. Comparison between predicted SWCC and results from this study (a) soil S8, and (b) soil S9.

degree of saturation (S) could also be keyed-in and the proposed equation still perform well. This is because while moisture content data of soils S1 and S2 (Fig. 8a and b), soils S6 and S7 (Fig. 11a and b), soils S8 and S9 (Fig. 12a and b) and soils S10 and S11 (Fig. 13a and b) are all in volumetric water contents. The moisture content data of soils S3, S4 and S5 (Figs. 9a and b and 10) are in the degree of saturation. Moreover, irrespective of the initial input in the solver, the equation will provide same output of variables, the only exception is that some equation's parameters sometimes in soil with a low liquid limit in this study, require manual updating after the usual best-fitting.

Conclusions

1. This work proposed a mathematical equation for modelling wetting bimodal SWCC. The proposed equation is accurate, with all its parameters having physical meaning in relation to the variables of the curve. A total of six (11) data set out of which five (5) are from published literature, and other six (6) experimental results from an engineered soil obtained by mixing different compositions of silty sand and inert kaolin, have been

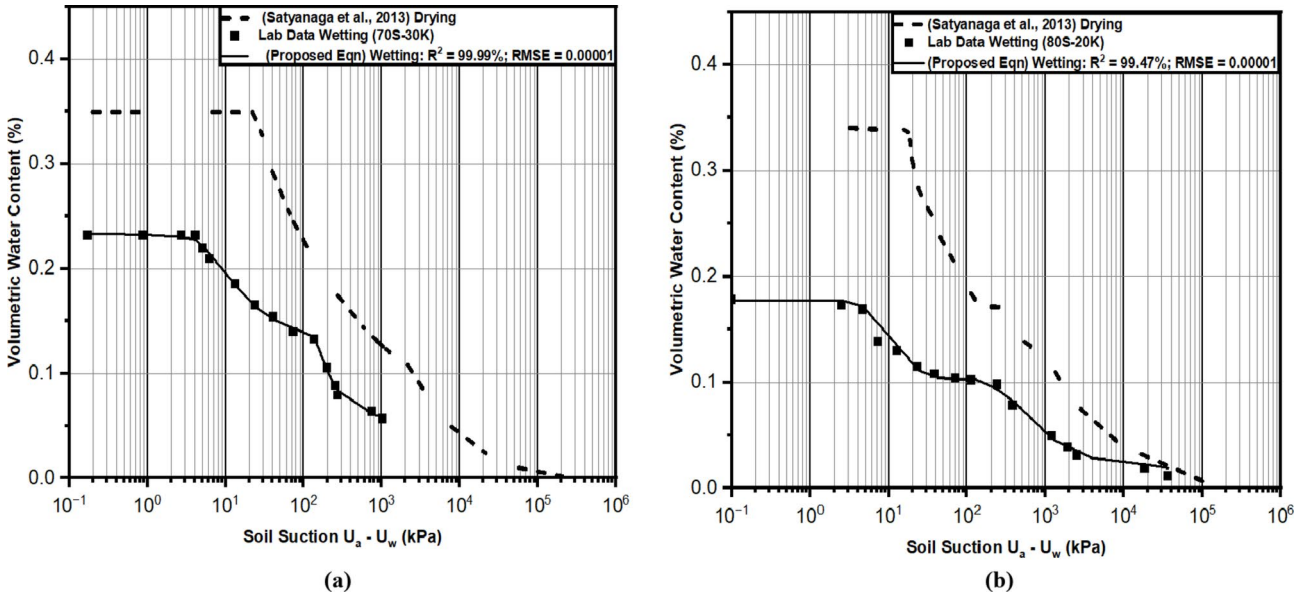

Fig. 13. Comparison between predicted SWCC and results from this study (a) soil S10, and (b) soil S11.

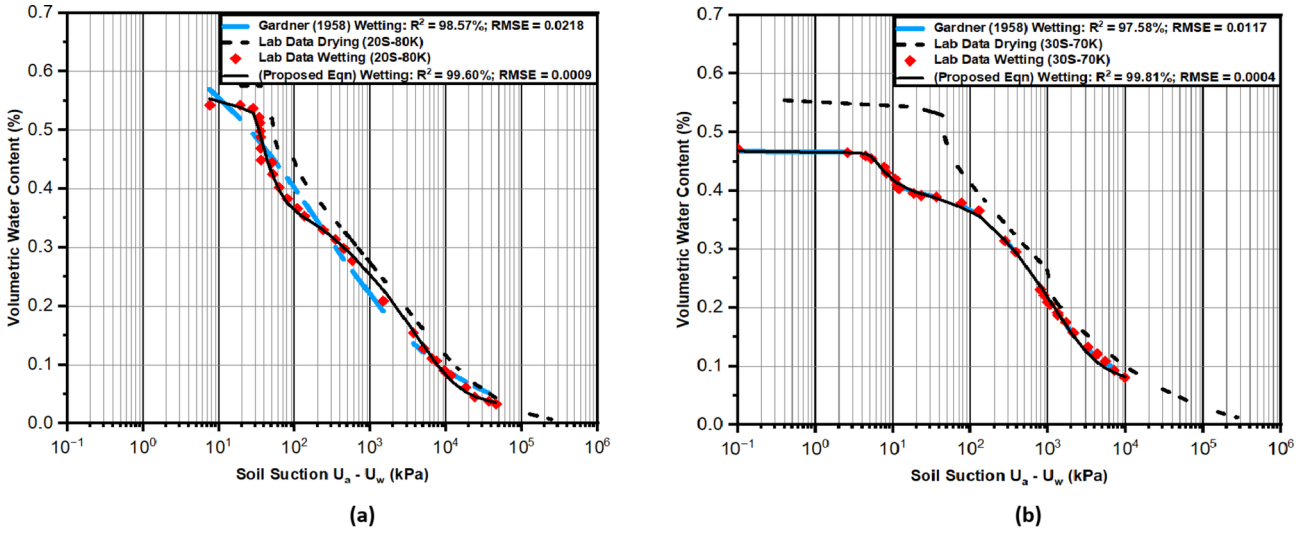

Fig. 14. Comparison between proposed model and Gardner (1958)[74] (a) Soil S6, and (b) Soil S7.

used to verify the performance of the proposed equation. The proposed equation has been verified with the said datasets using statistical method, the verification results show a significant performance of the proposed equation, with all the R^2 close to (1.0) and RMSE approaching (0.0).

2. Moreover, High Suction Polymer Sensor (HSPS) has only been used to measure drying SWCC in the past, a new approach to measure wetting SWCC using combination of HSPS, and dewpoint potentiometer (WP4C) has been developed in this work. The results obtained give bimodal SWCC that are quite similar to those obtained using other methods. Comparing this new method with the conventional methods such as the combination of Tempe Cell and WP4C, it can be concluded that this method provided more advantage of a shorter test duration.
3. The proposed model shows good performance as compared to results of laboratory tests on bimodal SWCC under wetting conditions, but some limitations and for a specific set of soils, however a number of limitations are identified as follows:

    a. Due to limitations in the availability of bimodal SWCC under wetting process in the literature, the model is validated using specific set of soil ranging from silty sand to coarse clay. More study on other soil samples outside this range is recommended.

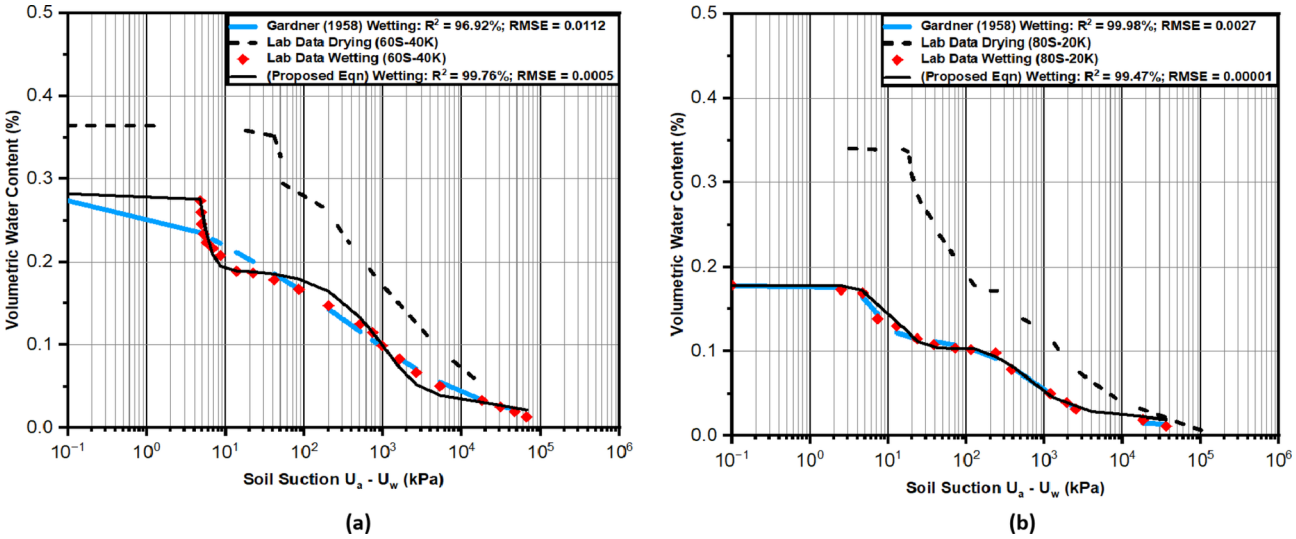

Fig. 15. Comparison between proposed model and Gardner (1958)[74] (a) Soil S9, and (b) Soil S11.

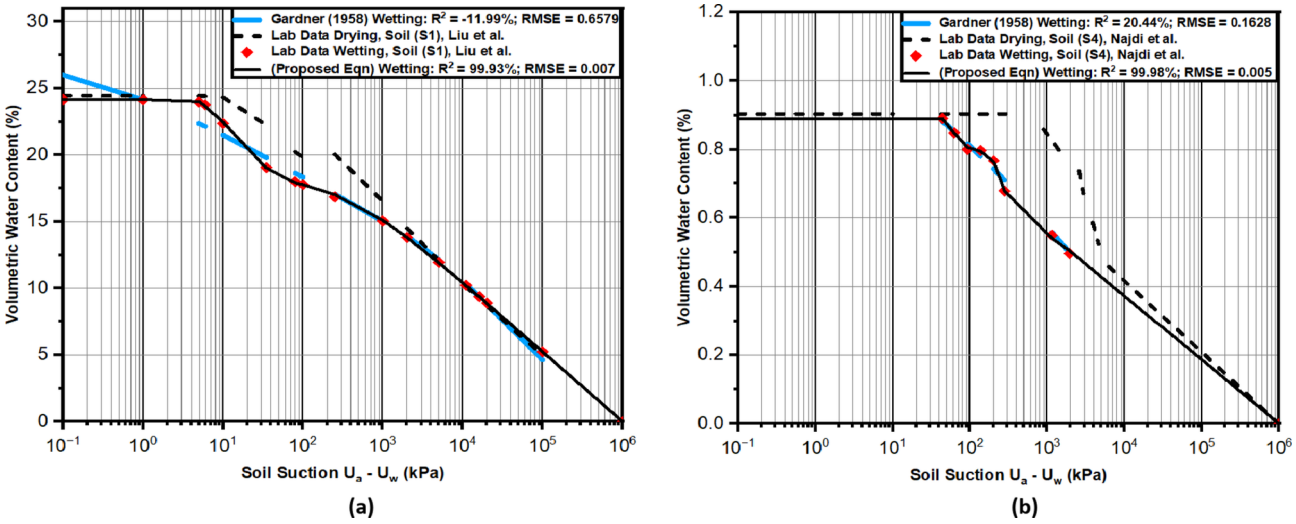

Fig. 16. Comparison between proposed model and Gardner (1958) equation[74] (a) Soil S1, and (b) Soil S4.

b. The effect of volume change is not considered, which might affect the model performance for soils with considerable volume change.
c. In an effort to keep the model as simple as possible, adding more parameters that may enhance the fitting ability especially in the transient part of the curve.
d. The simple scaling approach adopted in this study relies on the positions of key SWCC variables, as such, some intricacies of hysteresis such as ink-bottle effects are not fully captured.

Data availability

Data is provided within the manuscript.

Received: 6 January 2025; Accepted: 11 March 2025
Published online: 07 April 2025

References

1. Zhan, L., Chen, P. & Ng, C. W. W. Effect of Suction change on water content and total volume of an expansive clay. *J. Zhejiang University-SCIENCE A*. **8**, 699–706. https://doi.org/10.1631/jzus.2007.A0699 (2007).
2. Fredlund, D. G. & Xing, A. Equations for the soil-water characteristic curve. *Can. Geotech. J.* **31**, 521–532 (1994).
3. Vanapalli, S., Fredlund, D., Pufahl, D. & Clifton, A. Model for the prediction of shear strength with respect to soil Suction. *Can. Geotech. J.* **33**, 379–392 (1996).

4. Satyanaga, A. et al. Direct and indirect methods in determination of water retention curve of residual soils. In Proceedings of the 17th Asian Regional Conference on Soil Mechanics and Geotechnical Engineering (17th ARC), Astana, Kazakhstan, 14–18 August, CRC Press, 363–371. (2023). https://doi.org/10.1201/9781003299127-37
5. Du, C., Lu, X. & Yi, F. Impact of modifiers on soil–water characteristics of graphite tailings. *Sci. Rep.* **14**, 4186. https://doi.org/10.1038/s41598-024-52826-6 (2024).
6. Swanson, D., Savci, G., Danziger, G., Mohr, R. & Weiskopf, T. in *Tailings and Mine Waste*. 345–349.
7. Vanapalli, S. K., Fredlund, D. G. & Pufahl, D. E. The relationship between the soil-water characteristic curve and the unsaturated shear strength of a compacted glacial till. *Geotech. Test. J.* **19**, 259–268 (1996).
8. Li, C. et al. Estimation of the wetting induced settlement of loess soils from the wetting soil-water characteristic curve. *Sci. Rep.* **14**, 31533. https://doi.org/10.1038/s41598-024-83258-x (2024).
9. Pernebekova, G., Satyanaga, A., Abishev, R., Moon, S. & Kim, J. Water characteristic curve and permeability function of steel slag. In Proceedings of the 17th Asian Regional Conference on Soil Mechanics and Geotechnical Engineering (17th ARC), Astana, Kazakhstan, 14–18 August, CRC Press, 523–527. (2023). https://doi.org/10.1201/9781003299127-64
10. Qi, S., Vanapalli, S. K., Yang, X., Zhou, J. & Lu, G. -d. Stability analysis of an unsaturated expansive soil slope subjected to rainfall infiltration. *Geomech. Eng.* **19**, 1–9 (2019).
11. Satyanaga, A., Wijaya, M., Hamdany, A. H., Moon, S. W. & Kim, J. Green retaining structure utilizing recycled concrete aggregate. *Sustain. Mater. Civ. Infrastruct.*. https://doi.org/10.1016/B978-0-443-16142-1.00008-2 (2024).
12. Klausner, Y. *Fundamentals of Continuum Mechanics of Soils* (Springer Science & Business Media, 2012).
13. Satyanaga, A., Kim, J., Moon, S. W. & Wijaya, M. Exponential Functions for Modelling Hysteresis of Water Retention Curves. Proceedings of 4th European Conference on Unsaturated Soils. 19–21 October 2020, Lisboa, Portugal. (Web of Conferences). (2020).
14. Yang, H., Rahardjo, H., Leong, E. C. & Fredlund, D. G. Factors affecting drying and wetting soil-water characteristic curves of sandy soils. *Can. Geotech. J.* **41**, 908–920 (2004).
15. Prakoso, W. A. et al. Measurement of soil–water characteristic curve of vegetative soil using polymer-based tensiometer for maintaining environmental sustainability. *Environ. Sustain. Sustain.* **17**, 218. https://doi.org/10.3390/su17010218 (2024).
16. Pham, H. Q., Fredlund, D. G. & Barbour, S. L. A study of hysteresis models for soil-water characteristic curves. *J. C G J.* **42**, 1548–1568 (2005).
17. Zhai, Q. et al. A new domain model for estimating water distribution in soil pores during the drying and wetting processes. **322**, 107180 (2023).
18. Fredlund, D. G. Slope stability hazard management systems. *J. Zhejiang Univ-Sci A* **8**, 1695–1711. https://doi.org/10.1631/jzus.2007.A1695 (2007).
19. Wen, T., Luo, Y., Tang, M., Chen, X. & Shao, L. Effects of representative elementary volume size on three-dimensional pore characteristics for modified granite residual soil. *J. Hydrol.* **643**, 132006. https://doi.org/10.1016/j.jhydrol.2024.132006 (2024).
20. Burger, C. A. & Shackelford, C. Evaluating dual porosity of pelletized diatomaceous Earth using bimodal soil-water characteristic curve functions. **38**, 53–66 (2001).
21. Luo, Y., Wen, T., Lin, X., Chen, X. & Shao, L. Quantitative analysis of pore-size influence on granite residual soil permeability using CT scanning. *J. Hydrol.* **645**, 132133. https://doi.org/10.1016/j.jhydrol.2024.132133 (2024).
22. Wen, T., Chen, X., Luo, Y., Shao, L. & Niu, G. Three-dimensional pore structure characteristics of granite residual soil and their relationship with hydraulic properties under different particle gradation by X-ray computed tomography. *J. Hydrol.* **618**, 129230. https://doi.org/10.1016/j.jhydrol.2023.129230 (2023).
23. Zhanabayeva, A. et al. Comparative analysis of seismic design codes for shallow foundations adhering to the Kazakhstani and European approaches. *Sustainability* **15** (1), 615. https://doi.org/10.3390/su15010615 (2023).
24. Zhanabayeva, A., Moon, S. W., Kim, J. & Satyanaga, A. Comparative analysis of seismic design for shallow foundations adhering to the Kazakhstani and European approaches. In Proceedings of the 17th Asian Regional Conference on Soil Mechanics and Geotechnical Engineering (17th ARC), Astana, Kazakhstan, 14–18 August, CRC Press, 1614–1618. (2023). https://doi.org/10.1201/9781003299127-238
25. Wang, D., Li, C., Parikh, S. J. & Scow, K. M. Impact of Biochar on water retention of two agricultural soils–A multi-scale analysis. *Geoderma* **340**, 185–191 (2019).
26. Zhang, M. S., Chiu, C. F., Zhou, Y. Z. & Wang, Y. N. Compression and water retention behavior of saline soil improved by MICP combined with activated carbon. *Sci. Rep.* **14**, 31484. https://doi.org/10.1038/s41598-024-83083-2 (2024).
27. Zhou, J. & Jian-lin, Y. Influences affecting the soil-water characteristic curve. *J. Zhejiang University-SCIENCE A.* **6**, 797–804. https://doi.org/10.1631/jzus.2005.A0797 (2005).
28. Wen, T. W., Shao, P. & Guo, L. Experimental investigations of soil shrinkage characteristics and their effects on the soil water characteristic curve. *Eng. Geol.* **284**, 106035 (2021).
29. Fredlund, D. G. & Rahardjo, H. Unsaturated soil mechanics in engineering practice. *Can. Geotech. J.* **132**, 286–321 (2006).
30. Tripathy, S., Al-Khyat, S., Cleall, P., Baille, W. & Schanz, T. (2016).
31. Rahardjo, H. et al. in *Proc. 10th Australia New Zealand Conf. Geomechanics Common Ground*. 698–703.
32. Bello, N., Satyanaga, A., Aventian, G. D., Moon, S. W. & Kim, J. in *Smart Geotechnics for Smart Societies* 2378–2384CRC Press, (2023).
33. Gitirana Jr, G. & Fredlund, D. G. Soil-water characteristic curve equation with independent properties. *J. Geotech. Geoenvironmental Eng.* **130**, 209–212 (2004).
34. Kosugi, K. A new model to analyze water retention characteristics of forest soils based on soil pore radius distribution. **2**, 1–8 (1997).
35. Leong, E. C. & Rahardjo, H. Review of soil-water characteristic curve equations. *J. Geotech. Geoenviron. Eng.* **123**, 1106–1117 (1997).
36. Pedroso, D. M., Sheng, D. & Zhao, J. The concept of reference curves for constitutive modelling in soil mechanics. *Comput. Geotech.* **36**, 149–165 (2009).
37. Pedroso, D. M. & Williams, D. J. A novel approach for modelling soil–water characteristic curves with hysteresis. *Comput. Geotech.* **37**, 374–380 (2010).
38. Van Genuchten, M. A closed-form equation for predicting the hydraulic conductivity of unsaturated soils. *Soil. Sci. Soc. Am. J.* **44**, 892–898 (1980).
39. Amantay, A. N., Satyanaga, A., Moon, S. W. & Kim, J. Moisture sensing technology for assessment of rainfall-induced slope failure. In Proceedings of the 17th Asian Regional Conference on Soil Mechanics and Geotechnical Engineering (17th ARC), Astana, Kazakhstan, 14–18 August, CRC Press, 2042–2048. (2023). https://doi.org/10.1201/9781003299127-312
40. Zhang, L. & Chen, Q. Predicting bimodal soil–water characteristic curves. *J. Geotech. Geoenviron. Eng.* **131**, 666–670 (2005).
41. Li, Y. & Vanapalli, S. K. A novel modeling method for the bimodal soil-water characteristic curve. *Comput. Geotech.* **138**, 104318 (2021).
42. Tami, D., Rahardjo, H., Leong, E. C. & Fredlund, D. G. Design and laboratory verification of a physical model of sloping capillary barrier. **41**, 814–830 (2004).
43. Jiang, X., Wu, L. & Wei, Y. Influence of fine content on the soil–water characteristic curve of unsaturated soils. *Geotech. Geol. Eng.* **38**, 1371–1378 (2020).

44. Anandarajah, A. A. Priyanth microstructural investigation of soil Suction and hysteresis of fine-grained soils. *J. Geotech. Geoenviron. Eng.* **138**, 38–46 (2012).
45. Feng, M. & Fredlund, D. in *Proceedings from Theory to the Practice of Unsaturated Soil Mechanics in Association with the 52nd Canadian Geotechnical Conference and the Unsaturated Soil Group, Regina, Sask.* 14–20.
46. Confrey, J., Multiplication and Exponential Functions. *The development of multiplicative reasoning in the learning of mathematics* **291** (1994).
47. Zhao, Y., Rahardjo, H., Satyanaga, A., Zhai, Q. & He, J. A. General Best-Fitting equation for the multimodal Soil–Water characteristic curve. *Geotech. Geol. Eng.*, 1–14 (2023).
48. Coutinho, R., Silva, M. & Lafayete, K. in *Pan-Am CGS Geotechnical Conference.* 1–7.
49. Jotisankasa, A., Vathananukij, H. & Coop, M. in *Proceedings of the 4th Asia Pacific conference on unsaturated soils.* 263–268.
50. Orazayeva, S. et al. Advanced Scanning Technology for Volume Change Measurement of Residual Soil. Applied Science, 14, 10938. (2024). https://doi.org/10.3390/app142310938 (2024).
51. Rahardjo, H., Aung, K., Leong, E. C. & Rezaur, R. Characteristics of residual soils in Singapore as formed by weathering. *Eng. Geol.* **73**, 157–169 (2004).
52. Abishev, R. et al. Stability of soil slope in Almaty covered with steel slag under the effect of rainfall. *Sci. Rep.* https://doi.org/10.1038/s41598-024-58364-5 (2024). 14,7711.
53. Yeh, H. F. & Huang, T. T. L. Jhe-Wei. Effect of unimodal and bimodal soil hydraulic properties on slope stability analysis. *Water Resour. Res.* **13**, 1674 (2021).
54. Durner, W. Hydraulic conductivity Estimation for soils with heterogeneous pore structure. *Water Resour. Res.* **30**, 211–223 (1994).
55. Liu, Tang, L. & Chen, Y. Response of soil–water characteristics to pore structure of granite residual soils. *Soils Found.* **63**, 101395 (2023).
56. Najdi, A., Encalada, D., Mendes, J., Prat, P. C. & Ledesma, A. Evaluating innovative direct and indirect soil Suction and volumetric measurement techniques for the determination of soil water retention curves following drying and wetting paths. **322**, 107179 (2023).
57. Satyanaga, A., Rahardjo, H., Zhai, Q., Moon, S. W. & Kim, J. Modelling particle-size distribution and Estimation of soil–water characteristic curve utilizing modified lognormal distribution function. *Geotech. Geol. Eng.*, 1–19 (2023).
58. Li, X., Hu, C., Li, F. & Gao, H. Determining soil water characteristic curve of lime treated loess using multiscale structure fractal characteristic. *Sci. Rep.* **10**, 21569. https://doi.org/10.1038/s41598-020-78489-7 (2020).
59. Liu, Y., Shen, Y. & Jing, P. Study on the evolution characteristics and influencing factors of Frost heave on Kaolin clay during the horizontal freezing process. *Sci. Rep.* **15**, 187. https://doi.org/10.1038/s41598-024-84740-2 (2025).
60. ASTM-D2487-17. Standard Practice for Classification of Soils for Engineering Purposes (Unified Soil Classification System) 1. ASTM international, (2017).
61. ASTM-D6913M-17. *Standard Test Methods for particle-size Distribution (gradation) of Soils Using Sieve Analysis* (ASTM international, 2009).
62. ASTM-D4318-17. ASTM D4318-17e1: Standard Test Methods for Liquid Limit, Plastic Limit, and Plasticity Index of Soils. ASTM, (2018).
63. ASTM-D854-14. Standard test methods for specific gravity of soil solids by water pycnometer. ASTM international, (2006).
64. ASTM-D698-12. Standard Test Methods for Laboratory Compaction Characteristics of Soil Using Modified Effort (56,000 Ft-Lbf/Ft3 (2,700 KN-M/M3)) 1. ASTM international, (2009).
65. Fredlund, D. G. & Rahardjo, H. An overview of unsaturated soil behaviour. *Geotech. Spec. Publ. Eng. Geol.*, 1–1 (1993).
66. Van Der Ploeg, M. J. et al. Polymer tensiometers with ceramic cones: direct observations of matric pressures in drying soils. *Hydrol. Earth Syst. Sci.* **14**, 1787–1799 (2010).
67. Rahardjo, H. & Satyanaga, A. Effect of grain-size distribution on hydraulic anisotropy of unsaturated soils. Japanese Geotechnical Society Special Publication, 7(2), 376–381. Proceedings of 7th Asia-Pacific Conference on Unsaturated Soils (AP-UNSAT 23–25 August 2019, Nagoya, Japan. (2019) (2019).
68. Liu, H., Rahardjo, H., Satyanaga, A. & Du, H. Use of osmotic tensiometers in the determination of soil-water characteristic curves. *Geotechnique* **312**, 106938 (2023).
69. Leong, E. C., Tripathy, S. & Rahardjo, H. Total Suction measurement of unsaturated soils with a device using the chilled-mirror dew-point technique. *Geotechnique* **53**, 173–182 (2003).
70. Hatefi, M. H., Arabani, M., Payan, M. & Zanganeh Ranjbar, P. The influence of volcanic Ash (VA) on the mechanical properties and freeze-thaw durability of lime kiln dust (LKD)-stabilized Kaolin clayey soil. *Results Eng.* **24**, 103077. https://doi.org/10.1016/j.rineng.2024.103077 (2024).
71. Zhang, J., He, Z., Jiang, T. & Sun, D. a. Cone penetration model test of Xanthan gum-treated sand based on particle image velocimetry technology and its bearing capacity prediction model. *Environ. Earth Sci.* **84**, 19. https://doi.org/10.1007/s12665-024-12025-y (2024).
72. Satyanaga, A. et al. Water characteristic curve for soils in Kazakhstan. *Geotech. Eng. J. SEAGS AGSSEA*. **53** (4), 1–8 (2022).
73. Yeh, H. F., Huang, T. T. & Lee, J. W. Effect of unimodal and bimodal soil hydraulic properties on slope stability analysis. 13, 1674 (2021).
74. Gardner, W. Some steady-state solutions of the unsaturated moisture flow equation with application to evaporation from a water table. *Soil Sci.* **85**, 228–232 (1958).

Acknowledgements

This research has been funded by Nazarbayev University under Faculty Development Competitive Research Grant Program (FDCRGP) Grant No. 20122022FD4133. This research was also supported by Nazarbayev University Collaborative Research (CRP) Grant No. 111024CRP2014, Nazarbayev University Faculty Development Competitive Research Grant Program (FDCRGP) Grant No. 20122022FD4108 and Enterprise Development Grant (Co-innovation Program) BZ2023016 (Jiangsu) CIP-2207-CN1064 (Singapore). The authors are grateful for this support. Any opinions, findings, and conclusions or recommendations expressed in this material are those of the author(s) and do not necessarily reflect the views of Nazarbayev University.

Author contributions

Conceptualization: N.B., A.S., S.I.; Investigation: N.B., A.S., Q.Z.; Methodology: N.B., A.S., N.G.;Writing-original draft: N.B., A.S., S.I.; Supervision: A.S., N.G. J.K.; Funding acquisition: A.S., S.I.; Resources: Q.Z., N.G., J.K.; Data curation: N.B., S.I., Q.Z.; Validation: Z.Q., N.G.; Formal analysis: N.B., A.S., S.I.; Writing-review and editing: Q.Z., N.G., J.K.; Project administration: A.S., J.K.

Declarations

Competing interests
The authors declare no competing interests.

Additional information
Correspondence and requests for materials should be addressed to A.S.

Reprints and permissions information is available at www.nature.com/reprints.

Publisher's note Springer Nature remains neutral with regard to jurisdictional claims in published maps and institutional affiliations.

Open Access This article is licensed under a Creative Commons Attribution-NonCommercial-NoDerivatives 4.0 International License, which permits any non-commercial use, sharing, distribution and reproduction in any medium or format, as long as you give appropriate credit to the original author(s) and the source, provide a link to the Creative Commons licence, and indicate if you modified the licensed material. You do not have permission under this licence to share adapted material derived from this article or parts of it. The images or other third party material in this article are included in the article's Creative Commons licence, unless indicated otherwise in a credit line to the material. If material is not included in the article's Creative Commons licence and your intended use is not permitted by statutory regulation or exceeds the permitted use, you will need to obtain permission directly from the copyright holder. To view a copy of this licence, visit http://creativecommons.org/licenses/by-nc-nd/4.0/.

© The Author(s) 2025